

# Durable and Robust Solid Oxide Fuel Cells

**Hjelm, Johan; Hjalmarsson, Per; Knibbe, Ruth; Hauch, Anne; Graves, Christopher R.; Kiebach, Wolff-Ragnar; Curran, Declan; Frandsen, Henrik Lund; Ramos, Tania; Ebbehøj, Søren Lyng**

*Total number of authors:*
29

*Publication date:*
2012

*Document Version*
Publisher's PDF, also known as Version of record

# Index - Final Report - Project Results


1 Final report 2
1.1 Project Details 2
1.2 Executive summary 2
1.3 Project Overview and Milestones 4
1.4 Project Results 7
1.4.1 Durability of Solid Oxide Cells – A Literature Review 7
1.4.2 Work Package 1 - Materials and Cell Component Development.....9
1.4.3 Work Package 2 - Single Cell Testing 25
1.4.4 Work Package 3 - Development and Testing of Auxiliary Components.41
1.4.5 Work Package 4 - Cell and Materials Characterisation 44
1.4.6 Work Package 5 - Thermodynamic Calculations and Electrode Modelling 48
1.4.7 Dissemination of Project Results 50
1.4.8 Environmental Benefits of the Project 51
1.5 Utilization of project results 51
1.6 Project conclusion and perspective 52



*Report compiled by*: Johan Hjelm

*Contributors:* Per Hjalmarsson, Ruth Knibbe, Anne Hauch, Christopher R. Graves, Wolff-Ragnar Kiebach, Declan Curran, Henrik Lund Frandsen, Tânia Ramos, Søren L. Ebbe-høj, Mogens Mogensen, Alfred Samson, Martin Søgaard, Jonathan Højberg, Jacob R. Bowen, Karl Thydén, Peter S. Jørgensen, Sandrine Ricote, Rasmus Rode Mosbæk, Ming Chen, Sune Ebbesen, Vincenzo Esposito, Karen Brodersen, Anke Hagen, Jimmi Nielsen, Søren Foghmoes, Laila Grahl-Madsen, Bertil Sieborg, Johan Hjelm


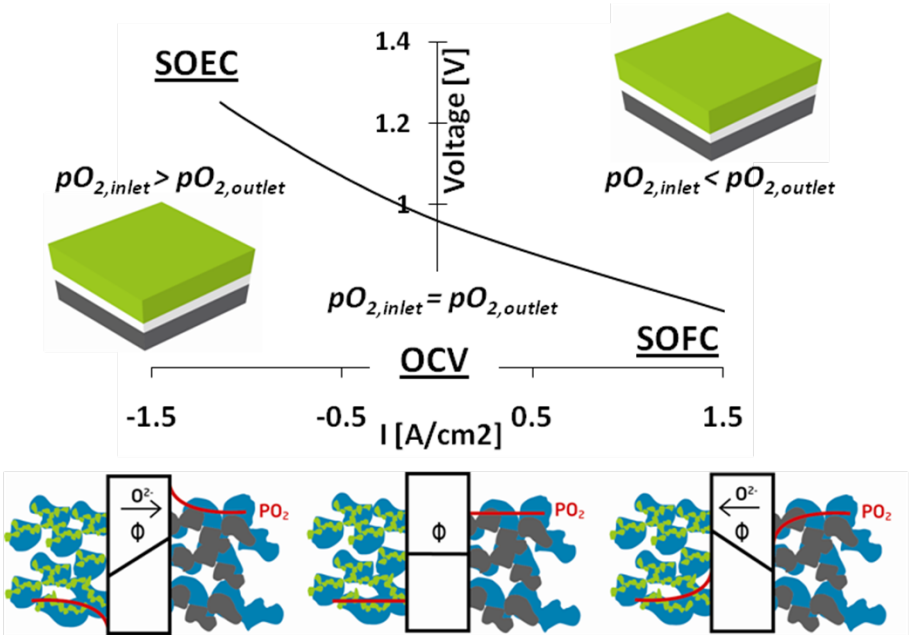

# 1 Final report

## 1.1 Project Details

| | |
|---|---|
| **Project title** | Durable and Robust Solid Oxide Fuel Cells |
| **Project identification** | Energinet.dk project no. 2010-1-10441 |
| **Name of the programme which has funded the project**<br><br>(ForskVE, ForskNG or ForskEL) | ForskEL |
| **Name and address of the enterprises/institution responsible for the project** | 2010-2011: Risø National Laboratory for Sustainable Energy (Risø DTU), Fuel Cells and Solid State Chemistry Division, Technical University of Denmark, Frederiksborgvej 399, 4000 Roskilde, Denmark<br><br>from 2012-01-01: Department of Energy Conversion and Storage, Technical University of Denmark, Risø Campus, Frederiksborgvej 399, 4000 Roskilde, Denmark |
| **CVR** (central business register) | DK30060946 |
| **Date for submission** | 2012-07-31 |

## 1.2 Executive summary

The solid oxide fuel cell (SOFC) is an attractive technology for the generation of electricity with high efficiency and low emissions. Risø DTU (now DTU Energy Conversion) works closely together with Topsoe Fuel Cell A/S in their effort to bring competitive SOFC systems to the market. This 2-year project had as one of its' overarching goals to improve durability and robustness of the Danish solid oxide fuel cells. The project focus was on cells and cell components suitable for SOFC operation in the temperature range 600 – 750 °C. The cells developed and/or studied in this project are intended for use within the CHP (Combined Heat and Power) market segment with stationary power plants in the range 1 – 250 $kW_e$ in mind. Lowered operation temperature is considered a good way to improve the stack durability since corrosion of the interconnect plates in a stack is lifetime limiting at T > 750 °C. The fact that degradation and robustness is not very well explored or understood at operating temperatures below 750 °C, provides motivation for focussing on materials and cells suitable for, and operated in this temperature range.

A significant part of this project was concerned with improved understanding of degradation and failure mechanisms. Improved understanding of performance and lifetime limiting factors will make it possible to develop strategies for counteracting degradation and improving the power density of SOFC based systems, both necessary to advance towards the goals set out in the national plan for SOFC implementation.

The project started with experimental activities along with a literature study reviewing the current status of degradation understanding. This lead to the publication of the review article "Durability of Solid Oxide Cells". The primary aim of this work was to collate and highlight the most pressing issues in degradation the area of solid oxide (fuel/electrolysis) cells. The

paper is split into five main focus areas – fuel electrode, oxygen electrode, electrolyte, cation diffusion and nano-particle degradation.

The development of new cells, cell components, and integration of new components into existing cell-platforms, *e.g.* the anode-supported Ni-YSZ half-cell: [Ni-YSZ(support)/Ni-YSZ(anode)/YSZ(electrolyte)], was undertaken in WP1, where the focus was placed on chemical and physical robustness of the fuel electrode, and alternative materials/structures for the oxygen electrode. Cells with different microstructures, and with variations in composition (*e.g.* ScYSZ/YSZ), were tested with respect to chemical and physical robustness. Some of the evaluation of the developed cells took place in WP2. This work lead to, among other things, improved understanding of the importance of microstructural differences between cells versus the difference in properties of the ionically conducting ceramic phase in Ni- cermet electrodes, a promising strategy for improvement of impurity tolerance (chemical robustness) of Ni-cermet electrodes in the form of nanostructured coatings, better insight into the impact of initial reduction of the Ni-cermet electrodes on their performance and stability, which is important for obtaining the best possible performance and durability from different types of cells. Furthermore a first assessment of the long-term stability of a cell with a nanostructured oxygen electrode was carried out, and LSC-based cathodes yielding excellent performance and promising long-term stability were developed and integrated into cells, that were also tested in the project.

In order to understand degradation better one needs to quantify the performance loss accurately, over sufficiently long times in cases where it cannot be accelerated in a meaningful way, and preferably in a component or process specific way. This has a number of consequences; 1) *physically reasonable models of the cell impedance*, i.e. the internal resistance of each cell, are needed in order to deconvolute the observed total cell impedance into specific resistance contributions - in particular under operation 2) *large amounts of data needs to be handled,* which in some cases amounted to several hundred impedance spectra for a single test 3) *auxiliary test components* (sealing materials, contact and gas distribution components used in test fixtures) that do not influence the stability of the cell and that does not generate systematic errors (such as additional resistance) in cell performance measurements are needed. These topics were dealt with within WP2 and WP3 in the project.

Development of a data analysis tool that is suitable for handling large amounts of data, including data quality validation tools, facilities for data analysis of complex impedance data using equivalent circuits and physical models - some which are not available in commercial software for this purpose. This development was supported by the project and took place within WP2. As a result, an improved description of degradation by detailed electrochemical characterization of cells operated at 0.5 - 0.75 $A \cdot cm^{-2}$ at 700 °C, in which the degradation (i.e. the change in performance) could be followed component or process-wise for periods of up to 3000 h, was obtained. The short and long-term degradation rates for different cell components, e.g. the Ni-YSZ anode, the YSZ electrolyte, and LSCF-CGO, LSC, and LSC-CGO cathodes were quantified.

Microstructural analysis and chemical analysis on the micro- to nano-meter scales was carried out within work package 4. This work package undertook development of methodology for chemical analysis in a scanning electron microscopy using samples manufactured with field-assisted ion beam milling, striking a compromise between resolution and relative ease of analysis. The project has also contributed to the development of software for extraction of quantitative microstructural information from electron microscopy micrograph *e.g.* phase fractions (porosity, oxides, *etc*) within WP4.

Work package 5 looked into the thermodynamic stability of the alternative, Sr-free, oxygen electrode material LCN, $La(Co,Ni)O_3$. A thermodynamic database of La-Co-Ni-O was developed, and thermodynamic calculations were then carried out to clarify the stability of LCN

cathodes as a function of temperature, Co/Ni ratio, and oxygen partial pressure. An impedance model was combined with a microstructural model and yielded a theoretical insight into how the impedance of anodes (Ni-cermet electrodes) should evolve as a function of time, assuming that nickel coarsening is the only factor contributing to the degradation.

The long-term degradation rates of the cells investigated in the project were in the range 6 – 16 $m\Omega \cdot cm^2$ per 1000 h and represents the intrinsic degradation rate of the cell, which is unavoidable (but most likely possible to improve further), and was obtained under steady-state conditions. This does not include extrinsic degradation (*e.g.* impurities in fuel or oxidant gas), degradation due to transient conditions, thermal cycles etc. Although the results indicate that there is little room for extrinsic degradation, these are promising results with respect to durability. The ASR is still too high with respect to the 2020 target. The outcome of this project provides guidelines for the future focus of development in order to achieve increased performance, better durability, and more cost-efficient anode-supported solid oxide fuel cells.

## 1.3 Project Overview and Milestones

The project was organized into five main activities (work packages, WP). They each addressed different aspects needed for the development of more efficient and durable cells. In WP1 improved cell components was developed and integrated into full cells. The cells were then electrochemically and mechanically tested in great detail (WP2) and characterized at the micro- and nano-scale (WP4). The results of testing and characterization were then fed back into the development work. Theoretical investigations of thermodynamic stability of a candidate oxygen electrode material (LCN) was undertaken in WP5, along with impedance modelling to aid the understanding of fuel electrode degradation (WP5). In WP3, auxiliary components needed for cell testing were developed and tested. In some cases the work packages were subdivided into work tasks (WT).

The work packages are listed below (Risø DTU is since 2012-01-01 DTU Energy Conversion):

WP1: Materials and Cell Component Development (Risø DTU)
WP2: Single Cell Testing (Risø DTU)
WP3: Development and Testing of Auxiliary Components (IRD A/S)
WP4: Cell and Materials Characterization (Risø DTU)
WP5: Thermodynamic Calculations and Electrode Modelling (Risø DTU)

Listed below are the milestones that were defined for the project and their status at completion of the project:

M1.1.1 - *A cell with an anode of improved chemical robustness developed and delivered for testing*
[Milestone fulfilled, delivery of cells with a Ni-ScYSZ cermet fuel electrode and ScYSZ electrolyte to WP2, this type of half-cell was tested for periods of up to 1000 h in two cases (with different oxygen electrodes) and showed very low degradation (< 1% per 1000 h) during operation in both hydrogen and in internally reformed methane. Ni-ScYSZ cermets electrodes have been shown to display greater tolerance to sulphur poisoning than Ni-YSZ cermets]

M1.1.2 - *A cell with an anode of improved physical robustness developed and delivered for testing*
[Milestone partially fulfilled. Cells previously made in smaller numbers (lab-scale) where up scaled and produced with industrially relevant production methods, *e.g.* tape-casting and screen-printing, and the cells were delivered for testing. A study of the tolerance of this cell type towards multiple fuel electrode redox cycles yielded no significant improvement in redox tolerance. Therefore this milestone is not considered to be met fully. However, the study did provide important new knowledge about the (microstructural) factors controlling redox stability and is therefore considered partially fulfilled.]

M1.2.1 - *Two alternative cathodes developed and tested*

[Milestone fulfilled. Several alternative cathodes (oxygen electrodes) were investigated, a composite LSC-CGO cathode, a pure LSC cathode, and composite LCN-CGO cathodes. LSC based cathodes were tested in detail, the influence of the ceramic raw materials (powders obtained from different suppliers) on manufacturing and performance was investigated, due to the high TEC of LSC studies of the tolerance of such LSC-based cathodes to thermal cycling was carried out. The performance of LSC based cathodes was generally very high, *i.e.* low polarisation resistances were observed.]

M1.2.2 - *Two cells with different nanostructured cathodes developed and delivered for testing*
[Milestone fulfilled. A half-cell with ScYSZ electrolyte and a Ni-ScYSZ cermet fuel electrode was selected as a platform for this work. The half-cell was integrated with a porous and ionically conducting layer of CGO on top of the electrolyte, and two series of cells were manufactured in which the porous backbone was infiltrated with electrocatalyst material from metal salt solutions to yield nanostructured electrodes with "LSC" or "LCN". It was observed that several phases resulted in each electrode, but the total composition of the electrocatalyst coating cor responded to that of the LSC or LCN particles used in regular composite electrodes. The cells were tested in WP2, and one of the cell types ("LSC") notably performed well and showed no net degradation during operation for 1000 h.]

M2.1.1 - *Installation of gas purification equipment in five SOFC test rigs*
[Milestone (revised) met. Two gas purification units were built and installed during the project, this milestone was revised from five to two units, due to a change in the perceived need, and more effort was placed on test methodology development instead.]

M2.1.2 - *Detailed electrochemical characterisation of the state-of-the-art 2.5G cell completed*
[Milestone fulfilled. The term "2.5G cell" refers to anode-supported cells of the composition [Ni-YSZ (anode) / YSZ (electrolyte) / CGO (protective barrier layer) / LSCF-CGO (cathode)] De tailed investigations of the cell impedance as a function of temperature, fuel and oxidant com position, and current density were carried out. Improved data analysis tools aided in identification of electrode and process specific contributions and improved physically reasonable models were implemented and used to separate the overall impedance into specific contribu tions, and to establish an accurate overpotential for each loss-process as a function of current density. This work laid the foundation for electrode and process specific degradation analysis of cells operating for more than 1000 h under current load.]

M2.1.3 - *Degradation rate of less than 1% per 1000h obtained in a 1500 h long-term test at 0.75 A·cm$^{-2}$*
[Milestone fulfilled. A cell has been tested under galvanostatic conditions (at 0.75 A·cm$^{-2}$) at 700 °C for a periods exceeding 1500 h. The anode-supported cells were of the composition [Ni-YSZ (anode) / YSZ (electrolyte) / CGO (protective barrier layer) / LSC-CGO (cathode)]. The protective barrier layer, preventing detrimental reaction between the cathode and the electrolyte, was deposited using physical vapour deposition. The initial degradation rate was significantly greater than 1% (with respect to initial cell voltage) per 1000 h. The resistance degradation rate over the last 2200 h of the test was 6.3 mV per 1000 h or 8.4 mΩ·cm²/kh. This corresponds to a relative degradation rate of 0.9% per 1000 h. Therefore this milestone is considered fulfilled.]

M2.1.4 - *Detailed electrochemical characterisation of a cell with an alternative cathode completed*
[Milestone fulfilled. Detailed investigations of the cell impedance as a function of temperature, fuel and oxidant composition, and current density were carried out. Improved data analysis tools aided in identification of electrode and process specific contributions. This work focused on cells with LSC-based cathodes, and the results were used for deconvolution of impedance spectra recorded during operation in order to generate a process specific degradation analysis.]

M2.1.5 - *Study of the effect of two different degradation mitigation strategies completed*
[Milestone met. Two potential degradation mitigation strategies were studied. Based on a previous observation at DTU Energy Conversion (previously Risø DTU) that indicated that extended dwelling at OCV (*i.e.* without DC bias) at operating temperature resulted in a lower degradation rate this strategy was selected for testing with respect to short-term/initial and long-term degradation. The second degradation mitigation strategy that was selected for

investigation was to address the "chemical robustness" of the Ni-YSZ cermet and involves modification of the material composition of the Ni-cermet electrode, either by addition of Sc to the ionically conducting phase (YSZ) or by modifying the internal surfaces of the cermet electrode with different kinds of (nanostructured) coatings. The latter strategy shows significant promise with respect to increasing the tolerance towards fuel gas impurities such as sulphur-containing species.]

M3.1 - *Evaluation of three different sealant materials as a function of temperature completed*
[Milestone fulfilled. Three different types of seals for single cell testing were tested as a function of sealing temperature. The seals tested can be divided into three types: Glass-based sealants, Metal/Alloy sealants, and compressive sealants. In general, the best results were obtained with sealants that were glass-based or metal/alloy based.]

M3.2 - *Development of simple manufacturing route for a low-temperature glass sealant component*
[Milestone fulfilled. Glass and Metal/Alloy based seals were manufactured by screen-printing of sealant containing inks on thin metal frames. The handling and manufacturing of such sealant frames is simple and less time consuming compared to the the state-of-the-art sealant glass bars used at Risø DTU.]

M4.1 - *Development and demonstration of a method for nano-scale analysis of SOFC electrodes using FIB-FEG-SEM*
[Milestone fulfilled. The aim of this work was to capitalise on the increased spatial resolution gained by using TEM type "thin" samples. In order to remove the time consuming process of performing in-situ TEM sample lift-out in the FIB-SEM an H-bar geometry sample was tested for its suitability for high resolution SEM EDS. Further work to reduce interfering signals from the thick surrounding parts of the H-bar sample the method was modified to create an asymmetric H-bar such that the thin section is raised to the top of the sample with respect to the incident electron beam such as "Π". This methodology, although more complicated than originally planned, was successful, and in comparison to conventional SEM bulk sample EDS analysis whose spatial resolution is approximately 1 µm, it can be concluded that the current technique offers approximately an increase in resolution of an order of magnitude.]

M5.1.1 - *Study of thermodynamic stability of LSCF-based cathodes as a function of temperature and oxidant gas composition completed*
[Milestone fulfilled after revision. As a concurrent PhD project was investigating the thermodynamic stability of LSCF, and results obtained in a previous project (ForskEL/PSO 2007-1-7124) on the performance of LCN – $La(Co,Ni)O_3$ used in composite SOFC cathodes, showed excellent performance and promising durability, this milestone was revised and the focus placed on LCN. A thermodynamic database of La-Co-Ni-O was developed, and thermodynamic calculations were then carried out to clarify the stability of LCN cathodes as a function of temperature, Co/Ni ratio, and oxygen partial pressure.]

M5.2.1 - *Clarification of origin of degradation based on impedance models*
[Milestone fulfilled. In order to improve the understanding of the degradation on both cells and model electrodes, different impedance models have been developed. The main focus was placed on the development of a physically reasonable impedance model of the anode response, as this is one of the components in the fuel cells that often shows the greatest total degradation, and the largest degradation rate at short times (< 1000 h). The developed impedance model was subsequently combined with a microstructural model, in order to quantify the effects on the impedance as a function of changing microstructural parameters in the anode. Specifically, this work investigated how the impedance of anodes should evolve as a function of time, assuming that nickel coarsening is the only factor contributing to the degradation.]

The main technical results within each activity, including accounts of the work related to fulfilling the project milestones, are outlined in the following section (1.3).

## 1.4 Project Results

Apart from work carried out to fulfil goals formulated as milestones in the project, a significant body of work has been carried out that aids in quantifying, understanding, and mitigating performance and lifetime limiting factors of Danish solid oxide fuel cell technology.

### *1.4.1 Durability of Solid Oxide Cells – A Literature Review*

The project started with experimental activities along with a literature study reviewing the current status of degradation understanding.[1] The literature study was co-financed by the Strategic Electrochemistry Research Center (SERC) This lead to the publication of the document "Durability of Solid Oxide Cells" The primary aim of this work was to collate and highlight the most pressing issues in degradation the area of solid oxide (fuel/electrolysis) cells. The paper is split into five main focus areas – fuel electrode, oxygen electrode, electrolyte, cation diffusion and nano-particle degradation. Initially a benchmark for an appropriate cell degradation is approximated and general terminology concepts are introduced. The paper attempts to collate cell durability concepts/data into palatable tables and figures. For example the driving forces for various degradation mechanisms can be understood from figure 1.

To maximise the lifetime of solid oxide (fuel/electrolysis) cells (SOCs) it is crucial to understand both intrinsic and extrinsic degradation related to the various cell components. For one component one set of cell operating conditions may be favourable to minimise one particular degradation phenomenon, but simultaneously may enhance another degradation phenomenon. Furthermore, it is imperative to establish a point of safe operation, where catastrophic degradation phenomena such as nickel oxidation and zirconate formation are avoided.

Over the past decades the understanding of solid oxide cell degradation has grown as can be evidenced by the large body of research. Although some cell/stack tests have shown that cell degradation is decreasing we are still not at a point where we can fully meet the strong commercial demands. Through the use of various essential tools such as electrochemical impedance spectroscopy and quantitative microstructural and chemical characterisation fundamental knowledge of SOC durability is being expanded, which is assisting in the development of new materials which are more tolerant to different types of degradation, and display a slower unavoidable degradation.

The various SOC degradation phenomena are dependent on SOC materials, processing and cell operating conditions. Parameters affecting the SOC durability during operation can be the operating temperature, current density, cell polarisation, the purity and type of gas supplied and fuel (and oxygen) utilisation. Different operating conditions lead to different oxygen activity profiles across the cell, which may affect the rate of the intrinsic degradation rate and in extreme cases corresponds to operation outside the "safe" operating parameter intervals. A schematic of the oxygen activity profile across the cell at different operating points is shown in figure 1.

Changes in performance with time can be grouped into *reversible* and *irreversible* degradation. To describe reversible performance loss or gain we use the terms *passivation,* and *activation,* respectively. To describe irreversible performance loss or gain we use *degradation,* and *irreversible activation,* respectively. In this project report, the term *'intrinsic'* phenomena will be used for SOC changes that occur due to the cell operating conditions, which phrased differently corresponds to unavoidable degradation, *e.g.* aging of materials and coarsening of microstructural features. The complementary term *'extrinsic'* degradation refers to SOC changes that occur as a result of external inputs such as feed gas impurities and emission of

[1] R. Knibbe, A. Hauch, J. Hjelm, S. D. Ebbesen, and M. Mogensen, *Green*, **1**, 141–169 (2011).

gas-phase impurities from auxiliary components (e.g. interconnects, seals, and balance of plant components).

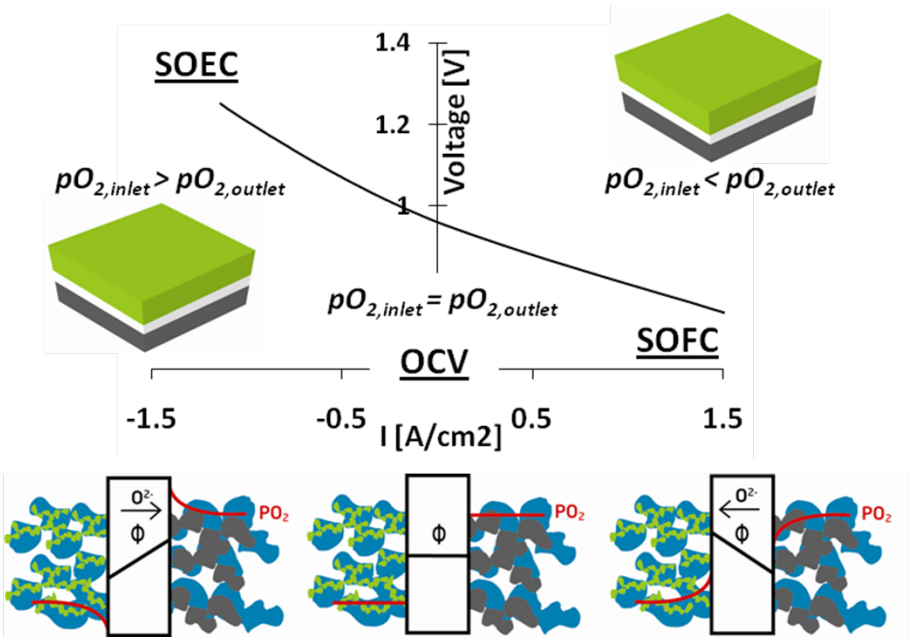


Figure 1: SOC current voltage curve with inset cross-section schematics showing the electrical and oxygen activity gradients in SOEC, OCV and SOFC case. Also fuel cell schematics indicate the oxygen partial pressure difference between the fuel electrode inlet and outlet.

### *1.4.2 Work Package 1 - Materials and Cell Component Development*

This work package had as its main objective to carry out ceramic processing research in order to enable manufacturing of new cell components and attempt integration of new cell components into full cells. The cell integration work in some cases also included components developed in other projects. The two focus areas were "Improved Robustness of the Anode", and "Improved Cathodes". By improved *chemical robustness* it is referred to the tolerance of the fuel electrode (solid oxide fuel cell anode) towards various impurities. By *physical robustness* it is referred to improved mechanical properties or improved tolerance to reduction-oxidation (redox) cycles of the Ni-cermet anode. Improving the solid oxide fuel cell cathode (oxygen electrode) was addressed by development of LSC-based $\{(La_{0.6}Sr_{0.4})_{0.99}CoO_{3-\delta}\}$ cathodes which display excellent performance, and investigation of other alternative cathode materials (free of Sr) such as LCN ($La_{0.99}Co_xNi_{1-x}O_{3-\delta}$) and LCCF ($La_{0.5}Ca_{0.5}Co_{0.8}Fe_{0.2}O_{3-\delta}$).

#### 1.4.2.1 - Development of Chemically Robust Anodes

Half-cells with Ni-ScYSZ anodes were supplied from another project and integrated with LSC and LSC:CGO cathodes, and delivered to WP2 for testing, hereby fulfilling milestone M1.1.1. Conventional Ni-YSZ based cells with CGO interdiffusion barrier layers and LSC and LSCF based cathodes were manufactured. The full cells were delivered to WP2 for performance and durability testing. Half-cells with Ni-ScYSZ cermet electrodes were tested to determine the intrinsic degradation rate of this type of cell by single cell testing in humidified hydrogen fuel ($H_2$:96%; $H_2O$:4%) and internally reformed methane with a slight excess of hydrogen ($H_2$ : 10% ; CH4:30%; $H_2O$:60%), compositions close to or identical to those recommended by the European projects FCTESTNet and FCTESqa.[2] Long-term testing of the 2.6G cell was conducted at 700 °C, 0.5 A·cm$^{-2}$, and at 60 % fuel utilization and 20% oxygen utilization. The results of the two tests are summarized in table 1, and figure 2 shows the cell voltage history plot for the tests.

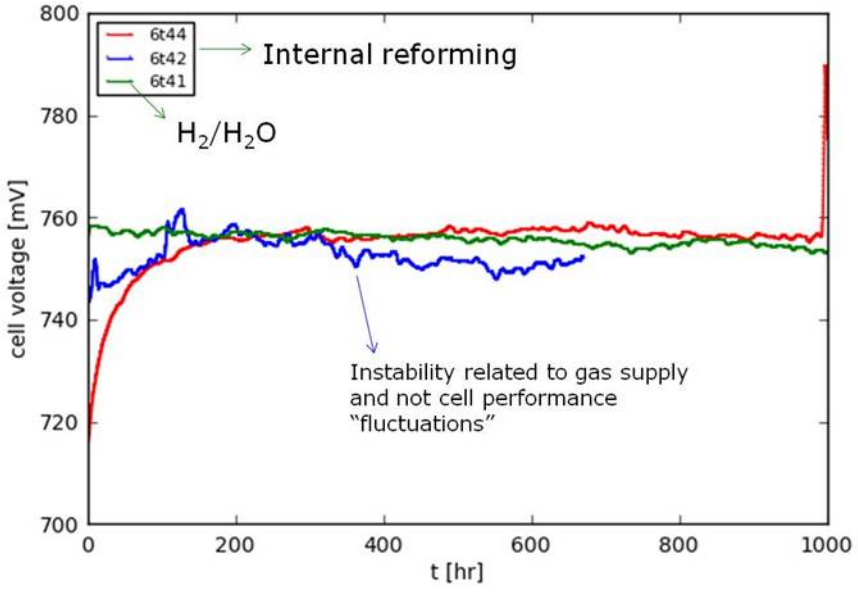


Figure 2: Cell voltage curves 2.6G cell tested at 700 °C, 0.5 A/cm$^2$, 4% $H_2O$ in $H_2$ (6test41) or 10% $H_2$ : 30% $CH_4$ : 60% $H_2O$ supplied to the anode at a flow rate corresponding to 60% $H_2$ utilization, and a mixture of 21% $O_2$ + 79% $N_2$ fed to the cathode at a flow rate yielding 20% oxygen utilization.

[2] see for example *JRC Scientific and Technical Report,* Test Modules TM SOFC 01-04LD / 05-08HD , http://iet.jrc.ec.europa.eu/fuel-cells/downloads-0

Figure 2 shows the cell voltage recorded as a function of time during up to 1000 h of fuel cell durability testing of three cells with Ni-ScYSZ cermet anodes and ScYSZ electrolyte. All cells had CGO barrier layers and LSC:CGO cathodes. The cell voltage only decreased from 757 mV to 753 mV; that is 4 mV/kh or 0.5 % voltage degr./kh (corresponding to an overall resistance increase of 8 mΩ·cm²/kh). *This provided one of the first indications of the good stability of the Ni-ScYSZ electrode (and the LSC:CGO composite cathode) at 700 °C and in both hydrogen and internally reformed methane fuel gas.* The increasing cell voltage in the beginning of 6test42 and 44 was due to a decreasing ohmic resistance and is thought to be due to a problem with the contact to the cells in these tests. These observations initiated work within WP2 to improve the cell test housing to yield more reproducible contact to the cell when using different cell types and different sealing and reduction temperatures.

Another activity within this work task examined the influence of variations in the ceramic processing parameters (mainly in the treatment of the raw powders before sintering) on the performance and durability of Ni-cermet fuel electrodes using symmetric cells as the test platform. The intention was to assess if moderate modification of powder chemistry, including surface properties, adhesion and sinter activity (through particle size changes) would influence the final microstructure significantly, thus performance or performance stability. To assess the impact on performance and short term stability under accelerated conditions of high steam, symmetric cells, with modified anode supports (Ni/3YSZ/additive) on both sides, were manufactured by tape-casting/lamination with the standard and modified anode tapes. Initial performance and the performance after short-term degradation (80 h at 850 °C) under very high steam contents (high steam content accelerates the short term degradation of Ni-cermets) was determined by electrochemical impedance spectroscopy. The impedance spectra have been analysed and compared using the polarisation resistance normalised distribution of relaxation times (DRT) calculated from the recorded impedance spectra. This has the advantage of capturing both the number of observed processes and their magnitude. Figure 3 shows the resulting plots from this series of investigations.

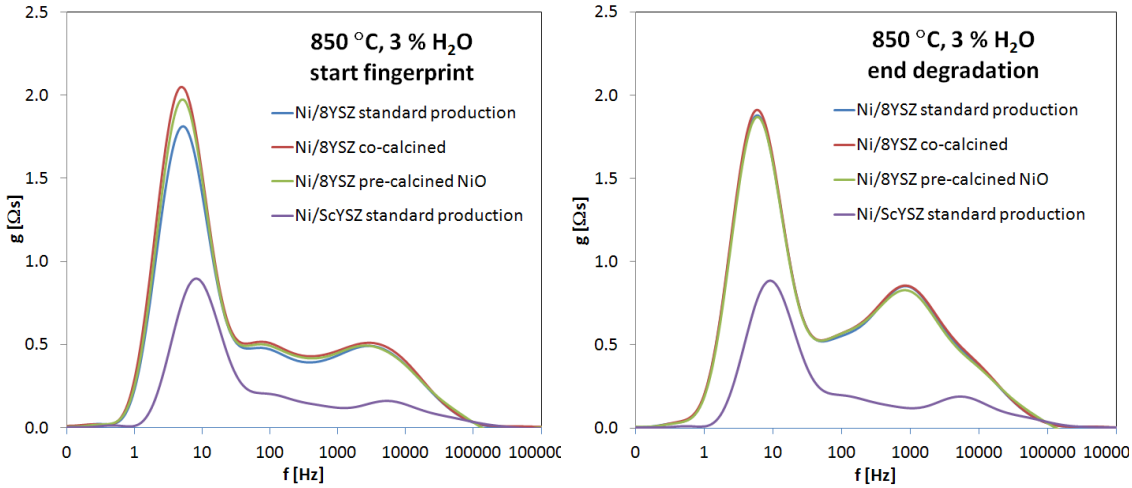

Figure 3: Comparative DRT plots for symmetric cells with Ni-(Sc)YSZ standard and modified production anodes at the start of the fingerprint and at the end of the degradation period in 80 % $H_2O$ in $H_2$ at 850 °C.

This effort showed no significant difference in the performance between the Ni-YSZ cermets, indicating that the powder pretreatments used here had negligible impact on the final product at the chosen processing and sintering conditions. Between the two different compositions differences are found both for the electrochemical part (> 100 Hz) and the gas transport related contributions (concentration polarisation, < 100 Hz). The electrochemical part of

teh Ni-ScYSZ is expected to be smaller due to the greater ionic conductivity of ScYSZ than YSZ, which allows the utilisation volume of the anode to expand and include a greater amount of reaction points (triple-phase boundaries), which has been reported by our group and others previously. The difference in gas transport properties is related to the difference in anode support density, which is greater for the Ni-YSZ sample due to the highersintering temperature used for this composition. The relative change in the electrochemical part of the polarisation resistance was smaller for the Ni-ScYSZ samples than for the Ni-YSZ samples, which indicates that the intrinsic degradation of Ni-ScYSZ is smaller than that of Ni-YSZ cermet electrodes. The origin of these differences are thought to lie in differences in contact angle and/or enhanced Ni-ceramic adhesion, similarly to what has been reported for Ni/Ti-doped 8YSZ cermets.[3]

Further investigations were carried out in order to provide a better understanding of the observed differences in the durability of cells manufactured in different ways (*e.g.* by spraying and by tape-casting) and with YSZ and ScYSZ in the active anode layer. Impurity build-up between Ni-particles, at triple phase boundaries (Ni/ionically conducting phase/gas phase), and between Ni particles and the ionically conducting ceramic phase (YSZ or ScYSZ) are all possible reasons for degradation, both long-term and short term. Ni-coarsening and/or roundening, both leading to a reduction in available triple-phase boundary, is well known to take place at relatively short times after initial reduction from NiO to form Ni and differences in the extent to which this takes place is possible in anode-cermets with differences in microstructure and/or surface energy of the ionically conducting ceramic phase.

Single cell testing of cells with sprayed anode layers (referred to as 2.0 G cells) and tape-cast anode layers (with ScYSZ in the anode layer and in the electrolyte, referred to as 2.X G cells) carried out within a previous project (ForskEL 2008-1-0065) has demonstrated a significantly improved stability of such 2.X G cells operated in humidified hydrogen at 750°C and 0.75 A $cm^{-2}$ as compared to 2.0G cells with YSZ in the active anode layer and the electrolyte. The 2.X G cell with ScYSZ was also shown to exhibit a significantly better tolerance to sulphur ($H_2S$) with internally reformed $CH_4$ as fuel (at 850°C and 1.0 A·$cm^{-2}$). In this project 2.0G cells (sprayed anode layer, YSZ in anode) and 2.XG cells (anode manufactured by tape-casting, both YSZ and ScYSZ versions) were explored in order to determine the importance of microstructural differences between the cells versus the importance of the difference in the properties of the ionically conducting ceramic phase. For example, YSZ displays a greater basicity than ScYSZ and the latter displays a greater conductivity than YSZ resulting in an expanded utilization volume in the anode under operation (i.e. a greater total amount of triple phase boundary is available to carry out the electrochemical oxidation of the fuel).

Cell testing was carried out on three types of cells, listed in table I along with relevant measured cell voltages, as well as its evolution over time, with and without the presence of 2 ppm of $H_2S$, for the three different cells described.

Table I: Cell voltages measured at start of FC testing at 850 °C, 140 l $h^{-1}$ air to the LSM-YSZ cathode, 1.0 A·$cm^{-2}$, internal reforming conditions for the anode (2.8 l $h^{-1}$ $CH_4$ , 5.6 l $h^{-1}$ $H_2O$ and 1.4 l $h^{-1}$ $H_2$), start of 2 ppm H2S exposure, inflection point for cell voltage curve during $H_2S$ exposure, and degradation from 125 h to 225 h of testing after starting $H_2S$ exposure.

| Cell type | Test no. | Start of FC 1 A/$cm^2$ | | Start of 2 ppm $H_2S$ | | Inflection point during $H_2S$ exposure | | Degradation 125 to 225 h after $H_2S$ on-set | |
|---|---|---|---|---|---|---|---|---|---|
| | | t (h) | U (mV) | t (h) | U (mV) | t (h) | U (mV) | $t_1 - t_2$ (h) | $U_1$-$U_2$ (mV) |
| 2.XG Ni/YSZ | **6t58** | 0 | 785 | 55 | 786 | 72 | 697 | 182-282 | 682-681= 1 |
| 2.0G | **4t40** | 0 | 681 | 73 | 674 | (128) | 570 | 198-298 | 543-517= 26 |
| 2.XG Ni/ScYSZ | **4t45** | 0 | 749 | 184 | 747 | 204 | 701 | 309-409 | 697-696= 1 |

[3] D. Skarmoutsos, P. Nikolopoulos, F. Tietz, I.C. Vinke, Solid State Ionics 170 (2004) 153.

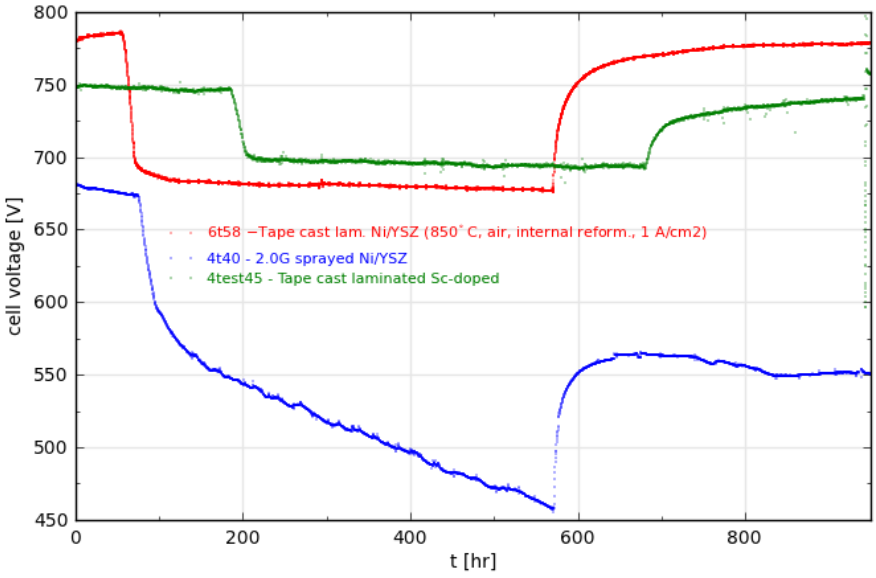


Figure 4: Cell voltage curves obtained at 850 ° C, 140 l $h^{-1}$ air to the LSM-YSZ cathode, 1.0 A·$cm^{-2}$, internal reforming conditions for the anode (2.8 l $h^{-1}$ $CH_4$, 5.6 l $h^{-1}$ $H_2O$ and 1.4 l $h^{-1}$ $H_2$. In the graph, t = 0 h correspond to start of testing under constant current load of 1 A/cm2 . 2 ppm $H_2S$ is added at t = 55 h, 73 h and 184 h, for 6t58, 4t40 and 4t45, respectively. See details in Table I. Cell voltage increase at t = 573 h, t = 684 h, and t = 580 h for 4t40, 4t45, and 6t58, respectively, is due to stopping of the 2 ppm $H_2S$ to the anode.

The cell voltage curves in figure 4 shows the difference in stability between the three types of cells. Compared to the 2.0G cell both 2.X G cells are significantly more stable, but the initial loss of cell voltage upon exposure to sulphur is greater in the 2.X G cell with YSZ than in the one with ScYSZ in the active anode. This initial loss of cell voltage is related to adsorption of sulphur on the Ni, and is greater for the cells with YSZ. However, the longer-term stability is similar for the two cells which were manufactured by tape-casting (the 2.XG cells). This indicates that both the chemical and physical properties of the ceramic phase is important for sulphur tolerance but that microstructural effects also are important, but mainly with respect to the timescale and magnitude of Ni-reorganization / coarsening. Figure 5 illustrates the current hypothesis regarding factors controlling durability of the anode Ni-cermet electrodes.

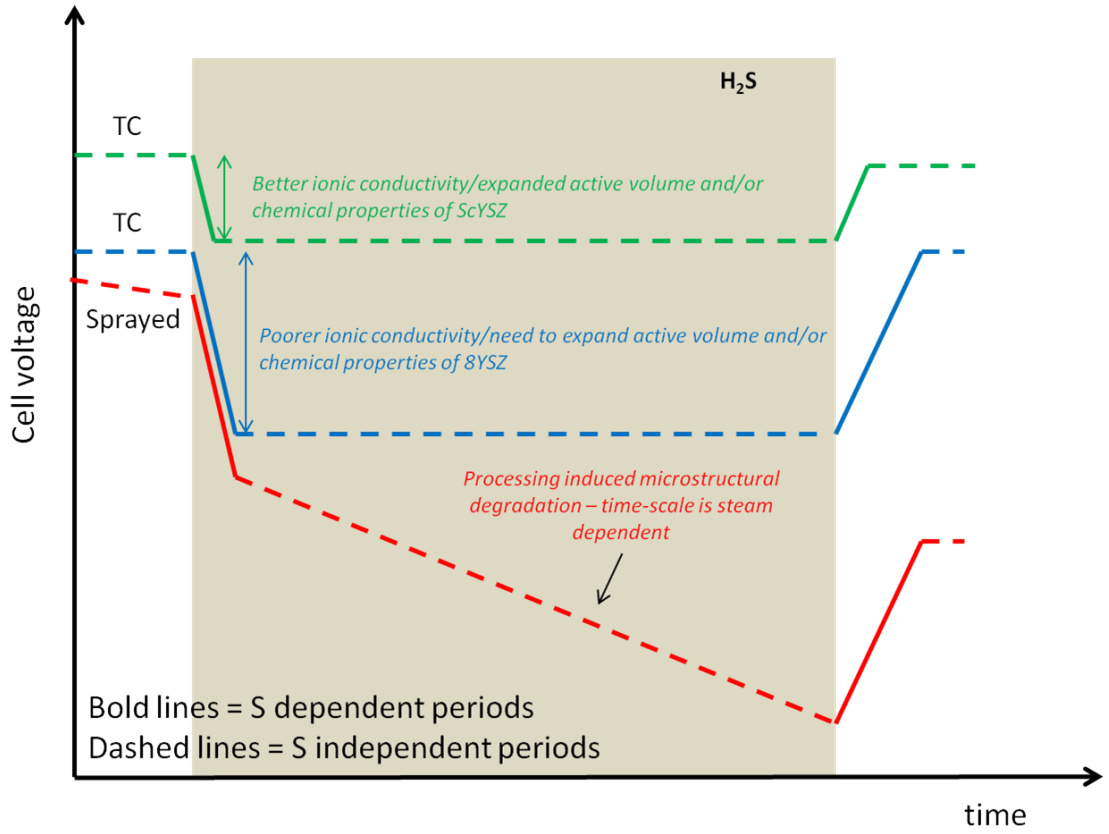


Figure 5: Schematic illustration of the current hypothesis surrounding sulphur-(in)tolerance of Ni/(Sc)YSZ cells processed in different ways. Degradation/recovery slopes are not necessarily based on experimental data, and should not be interpreted as such.

Although further tests are still clearly needed, this work has answered a very important question: enhanced robustness and impurity tolerance can be achieved by suitable processing (*i.e.* microstructural) modifications. Further studies should be able to determine the necessary processing/compositions/layer thickness combinations to maximise inherent S-tolerance, and establish how much more it is possible to decrease the intrinsic (microstructural rearrangement, coarsening etc) and extrinsic (additional degradation caused by poisoning, other gas phase impurities, or unfavourable operating conditions) degradation. Beyond this, infiltration of suitable additives in the anodes could provide further improvements to the impurity tolerance. An example of the latter strategy is discussed at the end of this section (see dicussion of results from the work to fulfill milestone M2.1.5).

The observations made in this project, earlier projects, together with reports in literature point to that the following three mechanisms control anode degradation in the absence of significant amounts of gas-phase poisons such as sulphur: all associated with loss of Ni percolation of sprayed Ni-YSZ anodes: a) increased Ostwald ripening (coarsening of particles) due to poor anchoring of the Ni particles on the ceramic matrix after initial reduction, which is time, temperature, and steam partial pressure dependent b) impurity build-up between Ni and the ceramic particles c) impurity build-up between Ni particles, disrupting the electrical percolation within the 'network' of Ni particles in the cermet electrode. Particle coarsening is expected to be important at relatively short times after reduction (within the first 100 - 1000 h of operation) while impurity buildup may take place over longer times, and conditions which increase mobility of impurities would in this case increase the degradation. Coarsening is a well established to take place in solid oxide fuel cell anodes, but the question is how important this particle growth is in relation to impurity effects and whether it is accelerated in

cases where the initial microstructure is such that one can describe the Ni anchoring as weaker, or when the Ni particle growth is hindered more or less by microstructural constraints.

The chemical composition of the tested 2.0G, and the two 2.XG cell versions (YSZ, ScYSZ) using energy dispersive x-ray spectrometry (EDS) in a scanning electron microscope (SEM) showed detectable amounts of Si, but the amounts were so low that quantitative analysis was not possible using this technique. Si-containing impurity films were identified between Ni and YSZ particles in the active anode of a 2.0G cell (see figure 6) , and although Si could be detected in both the YSZ and the ScYSZ versions of the 2.XG cell, no impurity rims were found between Ni and YSZ/ScYSZ in this case.

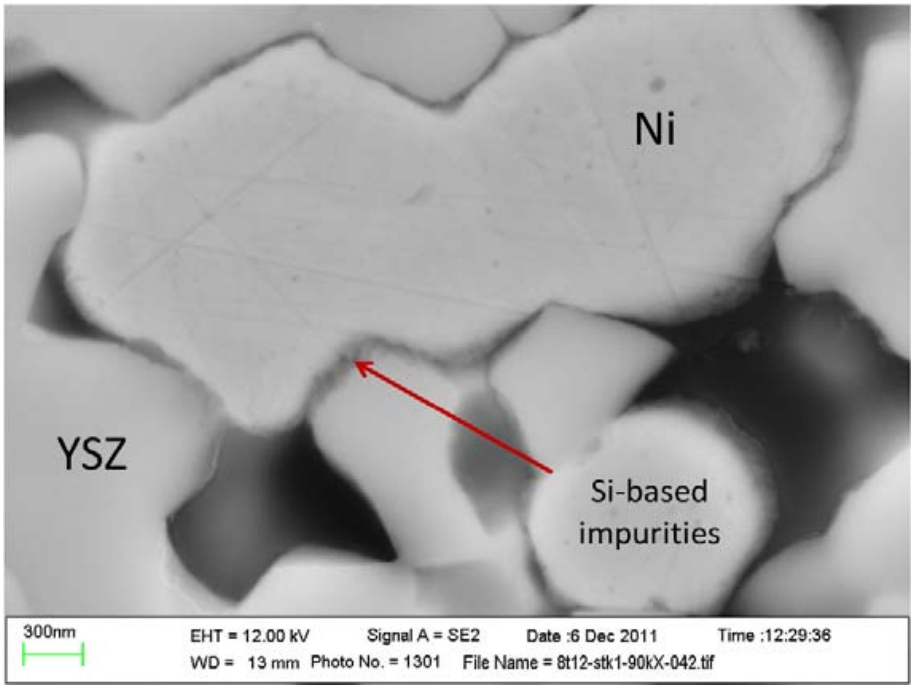


Figure 6: SEM micrograph showing accumulation of Si-based impurities between a Ni particle and a YSZ particle in the active anode layer in a 2.0G cell. The image was recorded using a tested sample.

These observations indicates that the explanation for the differences in stability between the cells 2.0G and 2.XG cells, may in part be due to impurity related effects (b and c).

The following work was part of the activities towards fulfilling milestone M2.1.5 - "*Study of the effect of two different degradation mitigation strategies*" and is the second of two main strategies investigated for mitigation of degradation. The results are reported under WP1 as the tests were carried out on symmetric cells and not on full cells, and that this strategy specifically addresses chemical robustness, *i.e.* tolerance towards fuel gas impurities.

The strategy investigated was to test modified material compositions of the Ni-YSZ electrode. One modification was the addition of Sc to the ion conducting phase during cell fabrication, yielding cells with Ni-10Sc1YSZ composite electrodes (described in other sections of this report). Another modification was surface modification of the composite electrode by infiltrating with additives, which form nanoparticles on the pore walls during calcination. Both methods offer the possibility to improve the tolerance of the Ni based electrode to impurities such as sulfur. Our initial results with surface modification showed that one infiltrated material is promising as a means to protect the Ni based electrode against poisoning – the electrode polarization resistance measured on symmetrical cells had negligible increase, compared with the reference cell without infiltrate and the other infiltrated materials (Figure 7). We are car-

rying on further research on this technique. *This technique is very promising in its potential to take existing Ni-based fuel-electrodes and simply add a coating that improves the electrode stability.* This strategy is expected to be explored further in future projects.

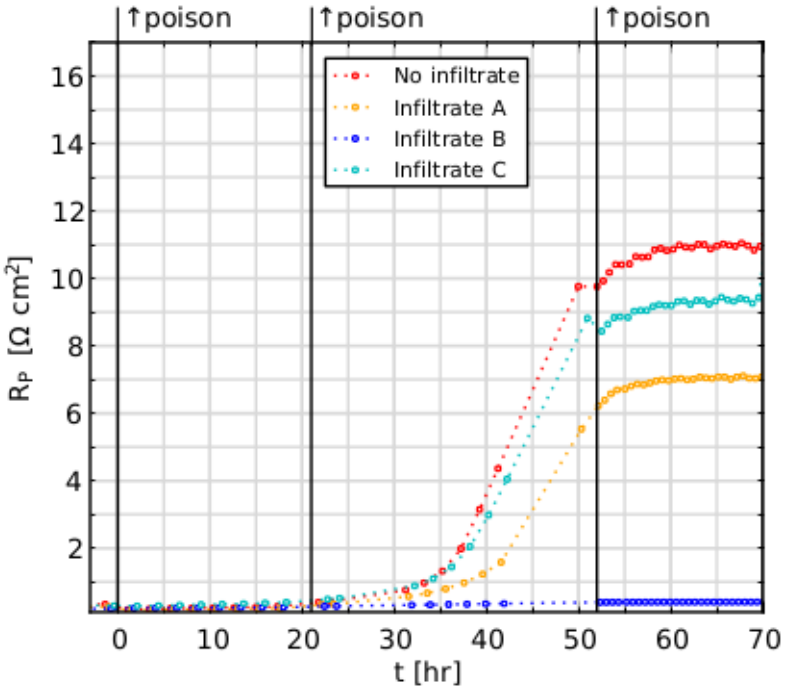


Figure 7. Initial results of infiltration of Ni based composite electrodes to form nanostructured coatings to prevent poisoning. The gas phase concentration of impurities was increased in (three) steps. $R_p$ is the total polarisation resistance of the symmetric cells.

### 1.4.2.2 - Impact of Initial Reduction Conditions on Performance and Stability of Ni-cermet anodes

The effect of various initial reduction procedures on the microstructure, performance and stability of Ni-ScYSZ cermet anodes was studied. A significant part of this work was conducted within a Master of Science project (S. L. Ebbehøj) supported by this project and that also resulted in a publication on this topic.[4] Additional work has since been carried out. Most of the porosity of Ni cermet anodes is produced via in-situ reduction of NiO, producing the electrically conducting network and significantly impacting the microstructure of the cermet. However, studies of the impact of reduction of Ni based cermet anodes on the microstructure and resulting performance of solid oxide fuel cells (SOFC) are few, and it is not clear from the available literature how the performance is affected by various reduction parameters, and how these should be chosen for obtaining optimal performance of the anode. In this work, two different anode reduction protocols were tested with regards to their impact on the electrochemical performance and stability of Ni-10Sc1YSZ and Ni-8YSZ anodes in anode supported symmetric cells by Electrochemical Impedance Spectroscopy and related to the obtained microstructure evaluated by Scanning Electron Microscopy (SEM) and Low Voltage SEM (LV-SEM). The aim was to identify the key parameters, assess their impact on, and optimise the procedure to further enhance, the performance and stability of Ni-ScYSZ electrodes. *This work also contributes to establishing methodology for low temperature reduction and start-up of full cell tests, which is necessary in order to study electrodes with nano-sized particles, produced by conventional ceramic processing or by use of infiltration techniques* (see for example M1.2.2).

[4] S. L. Ebbehøj, T. Ramos a and M. Mogensen , ECS Transactions, 2012, Volume 45, Issue 1, pp. 363-375

Reduction was done following two different protocols similar to those used at DTU for activation of full cells at high and low temperatures. These are named the High Temperature Full Cell (HTFC) and Low Temperature Full Cell (LTFC) protocols. Gas flows and temperature profiles of these protocols are summarized in Table II.

Table II. Parameters of two of the reduction protocols tested.

| Protocol | Ramp-up (>650 °C) | Annealing Steps | Reduction conditions |
|---|---|---|---|
| High Temperature Full Cell (HTFC) | Stagnant air: 60°C $h^{-1}$ | - Stagnant Air: 2h, 1000 °C<br>- 9% $H_2$ in $N_2$: 6 l/h, 2h | 3% $H_2O$ in $H_2$:<br>6 l/h, 1h, 1000 °C |
| Low Temperature Full Cell (LTFC) | $N_2$: 6 l/h, 60°C $h^{-1}$ | - $N_2$ (Ar): 6 l/h, 2h, 840 °C<br>- 9% $H_2$ in $N_2$: 6 l/h, 2h | Dry $H_2$:<br>6 l/h, 2h, 840 °C |

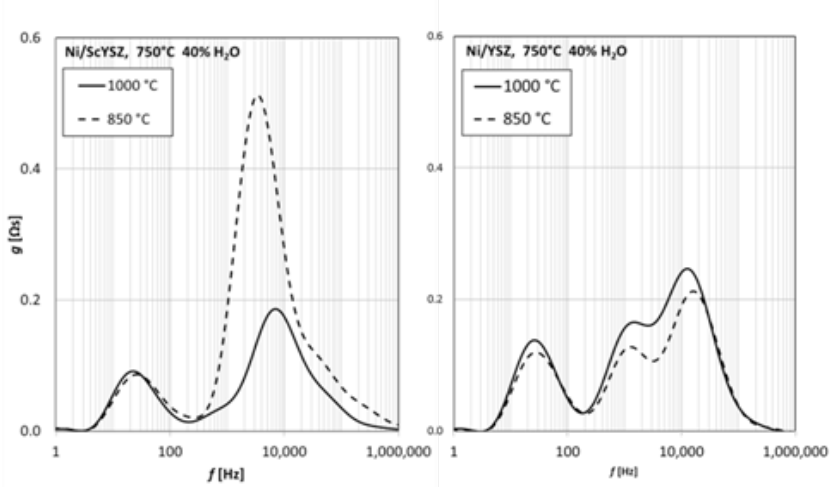


Figure 6: DRT analyses of EIS data obtained for Ni/ScYSZ (left) and Ni/YSZ (right) symmetric cells reduced by the HTFC (solid line) and LTFC ($N_2$) (dotted line) protocols as part of the stability tests.

The two types of cells were sintered at different optimum temperatures in the range of 1250-1350 °C, and spray coated with Ni/YSZ current collector layers. Following laser cutting to ~6x6 mm pieces, the cells were mounted in a custom built testing rig for symmetric cell testing. Following reduction impedance spectra were recorded and the corresponding DRT is displayed in figure 6.

From this first part of the study, it is clear that reduction at high temperatures in wet atmospheres produces lower electrode resistances than reduction at low temperature in dry atmospheres for Ni-ScYSZ cells, whereas the opposite is observed for Ni-YSZ cells. The difference is attributed to the greater interfacial adhesion in the Ni-ScYSZ system than in the Ni-YSZ system, hindering the microstructural changes needed for the formation of a good percolating Ni-network in the absence of steam and high temperatures. These conclusions were obtained under circumstances where the cells had been reduced at the temperatures of interest: 850 °C and 1000 °C, on fully or partially re-oxidised cells.

Analysis of the cermet electrodes after the different treatments show significant differences in the degree of electrical percolation in the Ni-phase and difference in the attachment of Ni-particles to the stabilized zirconia phase. Figure 7 shows micrographs illustrating the differences between Ni-YSZ and Ni-ScYSZ cermet electrodes.

Figure 7: a) SEM micrograph of Ni-ScYSZ / ScYSZ / Ni-ScYSZ layers after reduction using the HTFC protocol b) SEM micrograph of Ni-ScYSZ / ScYSZ / Ni-ScYSZ layers after reduction using the LTFC protocol

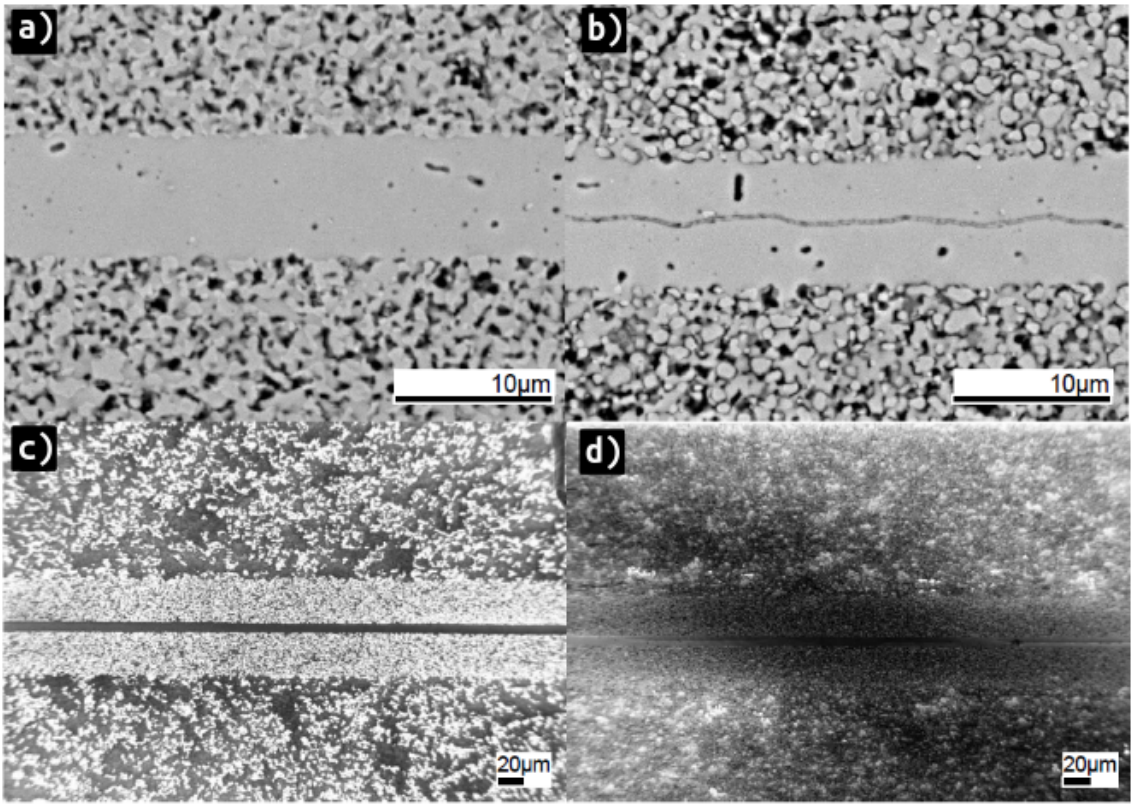


c) corresponding low acceleration voltage in-lens detection SEM image showing the percolating Ni-phase after reduction using the HTFC protocol and d) Ni-percolating phase in a sample reduced using the LTFC protocol.

Results from a thermogravimetric analysis (TA) study of Ni-cermet electrodes clearly show that near-complete reduction of Ni-ScYSZ cells at temperatures below 650 °C imposes severe morphological changes to the microstructure, characterised by the formation of seemingly "detached" Ni particles, porosity, or Ni particles with very poor wetting to the ceramic backbone. In this case, irreversible, almost complete loss of Ni percolation in the anode layer has been observed. Partial or full re-oxidation of the cells allows for full or almost full recovery of Ni-percolation, particularly in the presence of high steam contents. As the same phenomenon is not seen for Ni-8YSZ, it is speculated that it may arising from changes in the ScYSZ surface properties (*e.g.* dopant or impurity segregation to the surface of ScYSZ), that may be $pO_2$ and temperature dependent, leading to a different surface energy of the ScYSZ after treatment at high or low temperature and thus differences in the contact angle (wetting) of the Ni metal particles on the ScYSZ.

*A good understanding of the impact of the reduction of NiO to form the active Ni particle network in technical cermet electrodes is important in order to make sure that different cermet electrodes are utilized in the best possible way.* Future work in this area should address this issue in full cells, where both the effect of reduction on the initial cell performance and how it develops during operation should be explored further for different Ni-based cermet electrodes.

### 1.4.2.3 - Development and Testing of Physically Robust Anodes

The stability of the Ni-cermet fuel electrode towards cycles of re-oxidation and subsequent reduction, RedOx cycles, was addressed by investigation of parameters controlling redox stability in anode-supported cells. The range of cells tested are summarized in table III.

Table III: Cells investigated within RedOx tolerance study

*these anode supports have been modified to improve redox stability of the support

| Cell Type | Anode (A) | Anode thickness µm | Anode support (AS) | AS thickness µm | Electrolyte (E) | E thickness µm | Anode processing |
|---|---|---|---|---|---|---|---|
| 2.0G PS152795-1 | Ni/8YSZ | 8 | Ni/3YSZ | 322 | 8YSZ | 10 | Sprayed |
| 2.0G RR497 | Ni/8YSZ | 8 | Ni/3YSZ | 334 | 8YSZ | 10 | Sprayed |
| RDX-1 RDX-1-1 | Ni/8YSZ | 13 | Ni/3YSZ* | 306 | 8YSZ | 8 | Tape cast |
| RDX-2 RDSC-03-15 | Ni/8YSZ | 13 | Ni/3YSZ* | 296 | ScYSZ | 10 | Tape cast |
| 2.XG RR414-96 | Ni/ScYSZ | 24 | Ni/3YSZ* | 322 | ScYSZ | 6 | Tape cast |

Some of the key questions were a) the importance of the anode layer density / porosity, b) whether the redox stability is controlled by the anode layer or the anode support layer, and c) other key (microstructural) factors controlling redox stability. In order to estimate the porosity of the AFL and ASL after reduction, image analysis was performed using in-house developed software (see description of WP4 in section 1.4.5). Further, Hg intrusion porosimetry was also used to determine overall cell porosity, as well as average pore size and pore size distribution for each cell type.

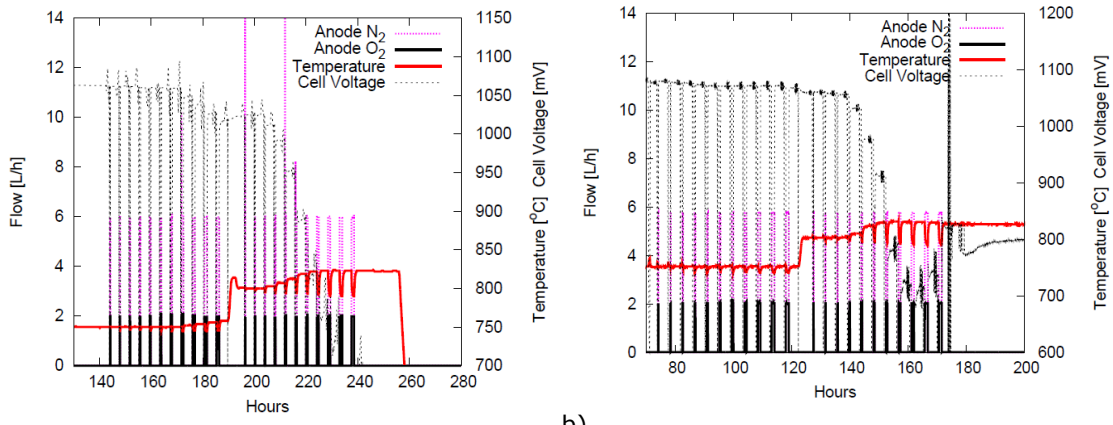


Figure 8: Cell voltage and temperature during RedOx stability tests of a) 2.0G cell (RR497) and b) of a RDX-1 cell.

The formation of cracks in the electrolyte is experimentally observed as a decrease in the cell voltage, concurrent with an increase in the cell temperature. The crack formation can also be seen in SEM micrographs of cross-sections of the tested cells. Failure of the cell occurs when the volume expansion in the anode layers, due to the Ni → NiO oxidation, becomes so large that it can no longer be mechanically tolerated by the electrolyte.

The anode side of the cells in this study were subjected to successively longer periods of oxidizing atmosphere, and the redox stability at 750°C was judged on how many cycles the cell could stand without any significant drop in cell voltage concurrent with an increase in cell temperature. Two representative data sets are illustrated in the graphs displayed in figure 8. Based on this data the redox stability at 750 °C was determined to be in the order (from greatest to poorest) RDX-1 > 2.0G > RDX-2 ≈ 2.XG. The difference between RDX-1 and RDX-2 is that RDX-1 has a custom anode support developed in a PhD project (M. Pihlatie, ”Stability of Ni-YSZ composites for solid oxide fuel cells during reduction and re-oxidation”, 2010)

which was carried out in collaboration between VTT, Finland, and Risø DTU, and later integrated into a cell and tested within the previous project (ForskEL 2008-1-0065) while RDX-2 had an anode support which was a first attempt to upscale the production of this anode-support, with a slightly modified particle size distribution, carried out in this project. The cell type RDX-1 was shown to be able to withstand the whole series of RedOx cycles at 750°C, without a significant change in cell voltage and cell temperature. The redox stability decreases with increasing temperature and also RDX-1 undergoes electrolyte failure after a few redox cycles at 800°C.

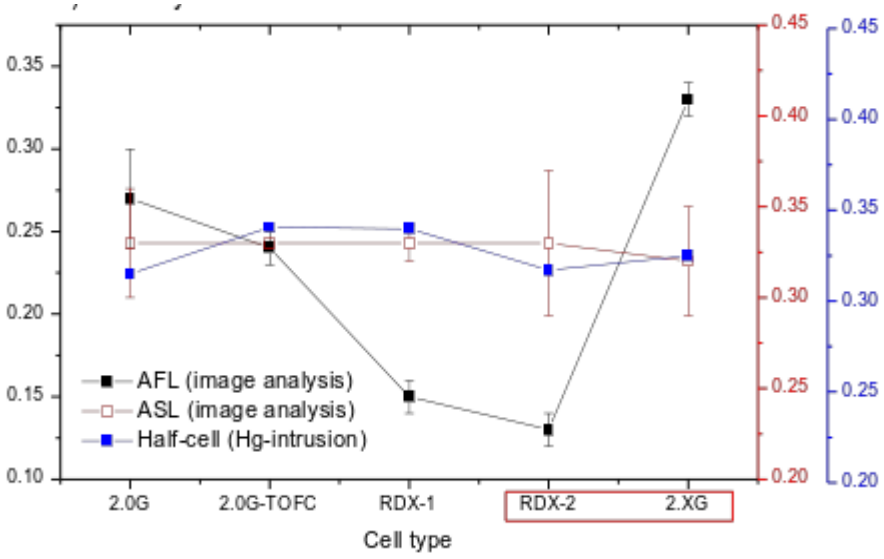


Figure 9. Measured porosities using Hg-intrusion porosimetry and quantitative image analysis of SEM micrographs of polished cross-sections of the investigated cell types.

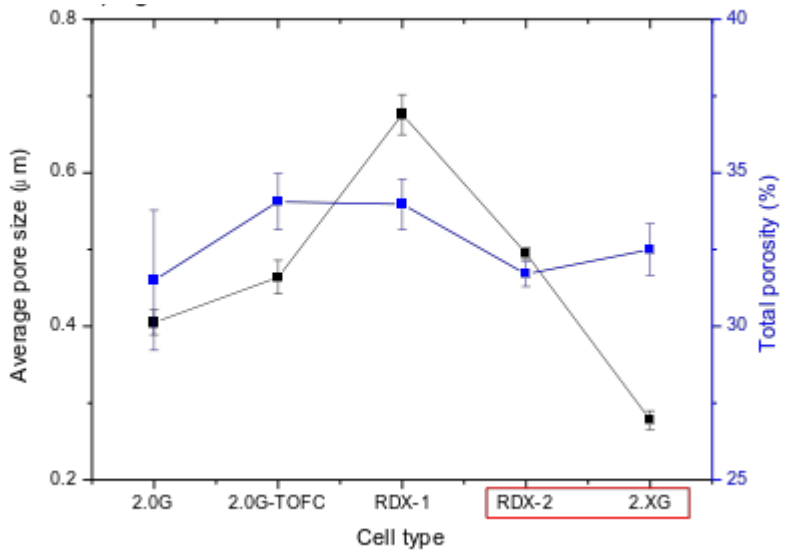


Figure 10. Total porosity and average pore size obtained using Hg-instrusion measurement on the investigated cell types.

The porosity data obtained for the anode and the support layer of all cells is illustrated in figures 9 and 10. The most notable differences between the cells lie in the porosity of the anode layer and in the average pore size of the anode supports used. The most redox stable cell (RDX-1) exhibits the largest average pore size in the anode support (> 0.6 µm) while all the other cells had average pore sizes near or below 0.5 µm. The total porosity of each half-cell determined by Hg-intrusion (corresponding to the anode support layer porosity as this layer

is about 20 times thicker than the anode layer) was not varying greatly between the cells when the experimental error is taken into account.

The two cells that exhibited the poorest redox stability (RDX-2 and 2.XG) displayed widely different porosity of the anode layer, which indicates that the support layer is more important than the anode layer with respect to controlling the redox stability of an anode supported cell. This is further supported by the observation that the most redox stable cell had a relatively dense anode layer. A greater average pore size in the support layer may accommodate volume expansion (upon reoxidation of Ni) better, and therefore lead to greater redox stability. This provides an important design parameter for introduction of greater RedOx stability in anode supported cells.

Thermogravimetric analysis of re-oxidation of half-cells indicate that the microstructural differences in the cells also may have a subtle influence on the re-oxidation kinetics, and is an issue that deserves more attention in the future.

The (well-known) fact that RedOx stability is improved at lower operating temperatures is connected to slower oxidation kinetics of Ni at lower temperatures, and thus a lower total degree of oxidation during a short RedOx cycle is another factor that is of technological importance, and highlights another benefit of decreased operating temperatures for anode-supported SOFCs.

*Although the upscale attempt in this project did not produce a physically more robust cell (RDX-2), the study carried out has provided better understanding of factors controlling redox stability and with this an important design parameter for more redox stable supports.* Milestone M1.1.2 ”A cell with an anode of improved physical robustness developed and delivered for testing” is thus considered only partially fulfilled.

RedOx stability is one of the targets mentioned in the national roadmap for SOFC implementation in Denmark (target for 2015). The work carried out in this project has provided understanding that can aid the effort to reach this target. The difficulty in transferring the lab-scale made cell (RDX-1) to a mass production friendly, upscaled, production (RDX-2) points to a relatively large cost/benefit ratio of the strategy of microstructural engineering as a pathway to reach the goal of RedOx stability, but further work in this area using the new knowledge may reduce this problem.

### 1.4.2.4 - Development and Testing of LSC-based Cathodes for Implementation in Solid Oxide Fuel Cells

As part of the effort to improve performance and durability of Danish anode-supported SOFC technology LSC-based cathodes have been further developed and investigated within the project. Both single-component LSC cathodes, and composite LSC-CGO cathodes were investigated. Some of the key concerns with LSC-based cathodes in the ontext of technological implementation are *i*) the relatively high thermal (and chemical) expansion coefficient (TEC) of this material with respect to that of the half-cell, *ii*) reproducibility of electrode performance and *iii*) long-term stability of cells with LSC-based cathodes. The first issue (the impact of TEC mismatch) was addressed by studying the change in in-plane conductivity and performance in symmetrical cells as a function of the number of thermal cycles the samples were subjected to in order to assess if any significant delamination or cracking of the LSC electrode layers took place as a consequence of thermally induced stresses. Reproducibility was investigated by manufacturing of electrodes using powders obtained from three different suppliers. Long-term stability was investigated using cells with single-component LSC cathodes and LSC-CGO composite cathodes, which is reported in more detail in sections X and Y.

Three different single-component cathodes with chemical composition $(La_{0.6}Sr_{0.4})_{0.99}CoO_{3-\delta}$ (LSC) have been prepared by manufacturing of inks and subsequenly screen printing the ceramic suspensions on dense self-supported CGO electrolyte tapes, followed by sintering. The electrodes were manufactured using similar, but not identical inks and ink components. The obtained symmetrical cells were then cut into 5*5 $mm^2$ samples and tested in a custom-built test rig. The obtained microstructures varied somewhat and for the two cathodes manufactured from the same powder (C, and D) the performance differed by a factor of two, indicating fair reproducibility even without thorough optimization.

The influence of thermal cycling was assessed using symmetrical cells [LSC/CGO/LSC] to investigate possible problems with delamination at the electrolyte-barrier layer interface. CGO has a TEC in the range 12 - $13 \cdot 10^{-6}$ $K^{-1}$ at 800 K, while YSZ has a TEC in the range 9-$10 \cdot 10^{-6}$ $K^{-1}$ at the same temperature, but considering that a Ni-YSZ cermet has a TEC in the range 11-12 $\cdot 10^{-6}$ $K^{-1}$ at 800K this is a technologically relevant experiment. The temperature profiles used are illustrated and the results of the electrical/electrochemical tests are illustrated in figures 11 and 12.

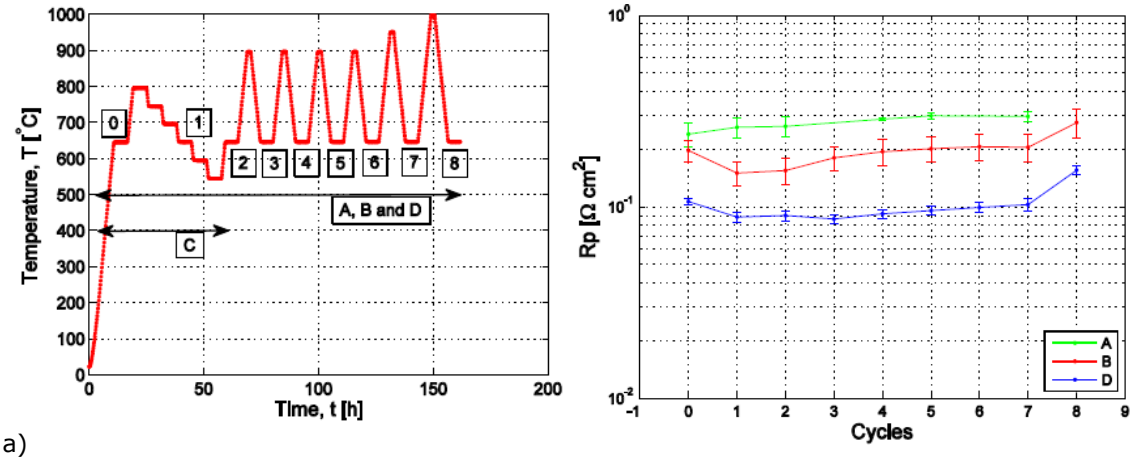


a) b)

Figure 11. a) Experimental T-profile used in the symmetrical cell test measurements b) Polarsiation resistance of three different cathodes (manufactured from different powders) plotted as a function of the measurement point number as indicated in a). All measurements were taken at 650 °C. Only the polarisation resistance is shown as delamination is expected to influence the series (ohmic) and the polarisation resistance in the same way.

The performance did not change significantly after thermal cycling in the (fairly limited) tempareture interval 600 - 870 °C. However, thermal excursions to 1030 °C caused an increased polarisation resistance, most likely due to coarsening of the electrode.

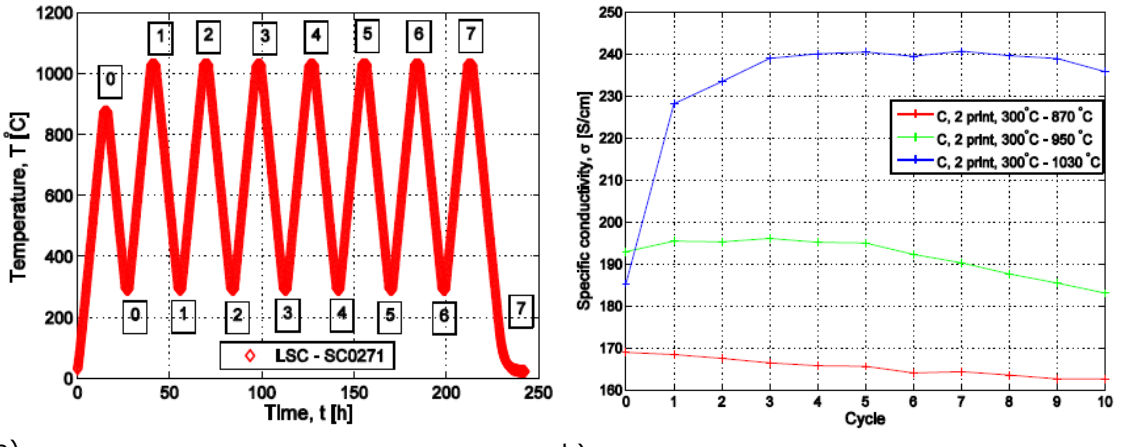


a) b)

Figure 12. a) Experimental T-profile used in the in-plane conductivity measurements b) In-plane conductivity data as a function of thermal cycle number within the given temperature ranges.

Future experiments of this kind should include a wider temperature interval with inclusion of lower temperatures (*e.g.* down to room temperature).

The structural integrity of LSC-based cells was investigated by monitoring the van der Pauw (vdP) in-plane conductivity of a 16 $cm^2$ electrode layer during thermal cycling in the temperature range 300 - 870, 950 or 1030 °C. When cycled to higher temperatures the conductivity increased, indicating further sintering of the cathode. *These initial experiments are promising with respect to maintained adhesion and structural integrity of LSC-based cathodes upon thermal cycling.* It should be noted that LSC-CGO composite cathodes, which show similar or better performance than the single-component cathodes tested here, are expected to have a lower TEC and therefore even better thermal stability.

The best LSC electrodes produced in the project yielded a performance (*i.e.* polarisation resistance) of about ~26 mΩ·$cm^2$ at 700 °C on symmetrical cells (excluding the gas diffusion resistance which is set-up related), and 34 mΩ·$cm^2$ at 700 °C on full cells (e.g. cell A at 0.5 A $cm^{-2}$ in section 1.4.3.4). The best LSC-CGO composite cathodes manufactured in this project had lower polarisation resistances of < 20 mΩ·$cm^2$ at 700 °C, measured at OCV on symmetrical cells, a value the correlates well with that observed in full cell tests. Representative symmetric cell test measurements are displayed in figure 13. These values are significantly lower than the resistances observed for the tested LSCF-CGO cathodes under similar conditions (~50-100 mΩ·$cm^2$ at 700 °C).

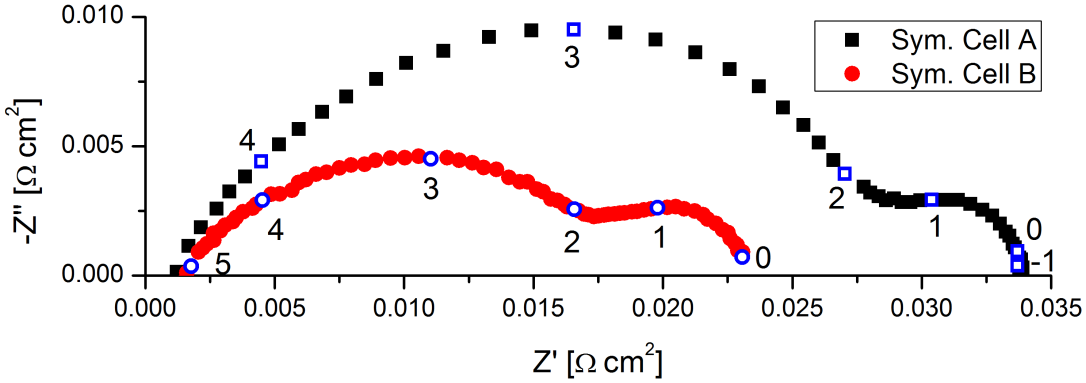


Figure 13. Nyquist plots of the impedance measured on symmetric cells in air at OCV and 700 °C with the same cathodes as those applied to Cell A (LSC) and Cell B (LSC-CGO) in section 1.4.3.4. Integers denote $\log_{10} f$.

The LSC cathodes developed within this activity were integrated on full cells and tested to determine the performance and durability on full anode-supported cells within WP2. The results are reported in more detail in section 1.4.3.4. The milestone M.1.2.1 "Two alternative cathodes developed and tested" is considered fulfilled as four different cathodes LSC, LSC-CGO, LCN-CGO, and LCCF were developed and tested (the latter two are described in section 1.4.2.5) with two of these (LSC, LSC-CGO) giving excellent results with respect to performance, and as reported in section 1.4.3.4, also very good stability under operation with current load.

### 1.4.2.5 - Investigations of Sr-free Cathode Materials

An alternative (Sr-free, but with a smaller alkali earth ion; $Ca^{2+}$ instead of $Sr^{2+}$) cathode

was made from the promising alternative cathode material LCCF ($La_{0.5}Ca_{0.5}Co_{0.8}Fe_{0.2}O_{3-\delta}$), a material that shows high oxygen exchange rate and is a mixed conductor – very similar to LSC and LSCF. However, the tests showed that this material is problematic to integrate on 2.5/2.6G half-cells due to the rapid interdiffusion of the A-site dopant $Ca^{2+}$ through the protective CGO barrier layer. Figure 14 shows micrographs of a polished cross-sections of a cell with a screen-printed and sintered LCCF cathode. A thin reaction layer is visible between the electrolyte and the barrier layer, which was confirmed to be rich in Ca by energy dispersive X-ray spectroscopy (EDS). The results show that CGO barrier layers are not sufficient barriers to prevent $Ca^{2+}$ interdiffusion and reaction between the cathode and the electrolyte. *The high solubility of $Ca^{2+}$ in ceria (reported in recent literature) and the significantly greater overall diffusion of $Ca^{2+}$ than $Sr^{2+}$ makes LCCF unsuitable for 2.5G and 2.6G type cells, which both rely on a protective CGO interdiffusion barrier layer.* Due to these findings development of LCCF as an SOFC cathode was discontinued within this project.

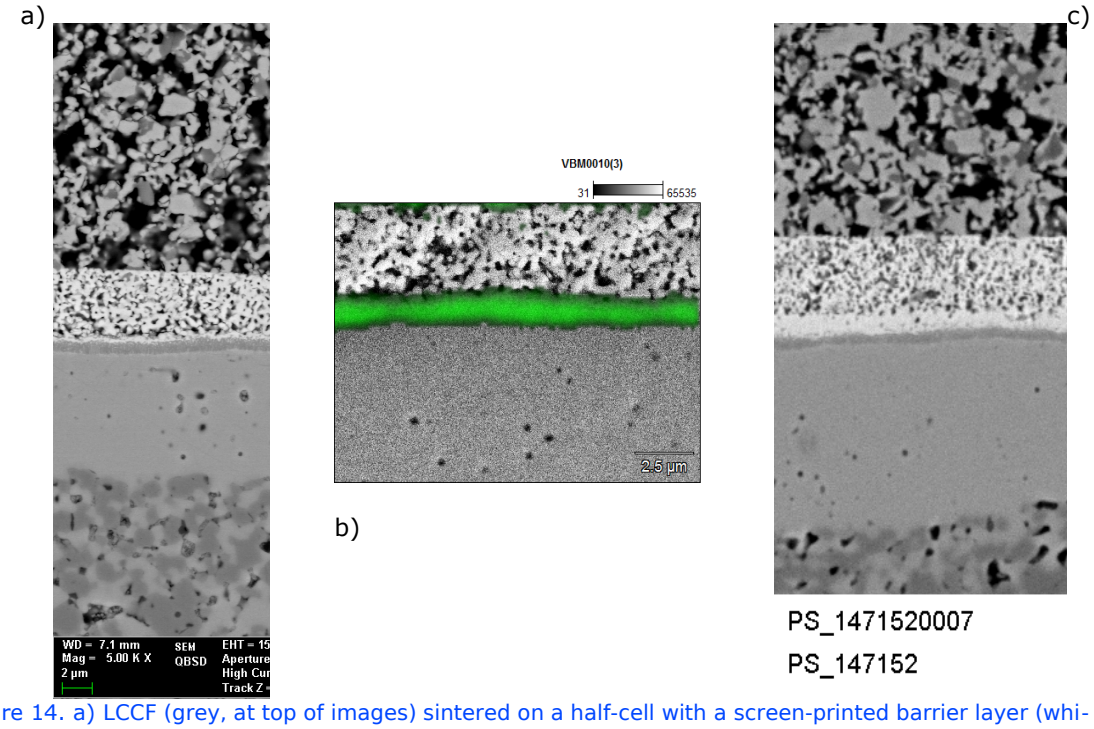


Figure 14. a) LCCF (grey, at top of images) sintered on a half-cell with a screen-printed barrier layer (white porous layer), b) EDS map of barrier – reaction layer – electrolyte. The green color intensity indicates the amount of Ca present. c) LCCF sintered on top of a screen-printed barrier deposited on a spin-coated barrier layer (for improved diffusion barrier properties). In both cases the interdiffusion barrier properties of the CGO layers were insufficient, and a reaction layer was present between the electrolyte and the barrier layer.

Another alternative oxygen electrode material that was investigated in the project was $La_{0.99}Co_{1-x}Ni_xO_{3-\delta}$ (LCN). Results obtained in a previous project (ForskEL/PSO 2007-1-7124) on the performance of LCN – $La(Co,Ni)O_3$ used in composite SOFC cathodes showed excellent performance.[5] $LaCo_{1-x}Ni_xO_{3-\delta}$ (LCN) with x=0.4-0.6 has been reported to possess high electronic conductivity and a thermal expansion coefficient (*TEC*) that is relatively well matched to a SOFC. Yet it has still received surprisingly little attention in the context of SOFC electrode material. The major drawback of this material is the low oxide ion conductivity that restricts the use of LCN as a single phase electrode. Therefore, in order to work efficiently as an electrode at relatively low operating temperatures, it is necessary to mix it with an oxide ion conductor such gadolinia doped ceria (CGO).

The aim of this activity was to reproduce this electrode and integrate it on a anode-supported half cell with a CGO barrier layer in order to investigate the long-term stability of this material

[5] P. Hjalmarsson and M. Mogensen, *Journal of Power Sources*, **196**, 7237–7244 (2011)

when used as oxygen electrode. Symmetrical cell test results presented in [5] indicated good stability of this material. Powder from two different sources was tested the influence of sintering temperature and manufacturing reproducibility was investigated.

The results showed that neither of the produced cathodes reproduced the good electrochemical results of the first cathode (ink id# SC0113) made previous to this project, both the polarisation and the ohmic resistance as determined by symmetrical cell testing was significantly greater than that observed for the original electrode in all three cases. The reference samples reported in [5] were measured again in order to verify that the electrochemical performance was correctly measured. It was found that the resistance this time was slightly higher than what was first reported but still about one order of magnitude lower than for the electrodes developed within this project.

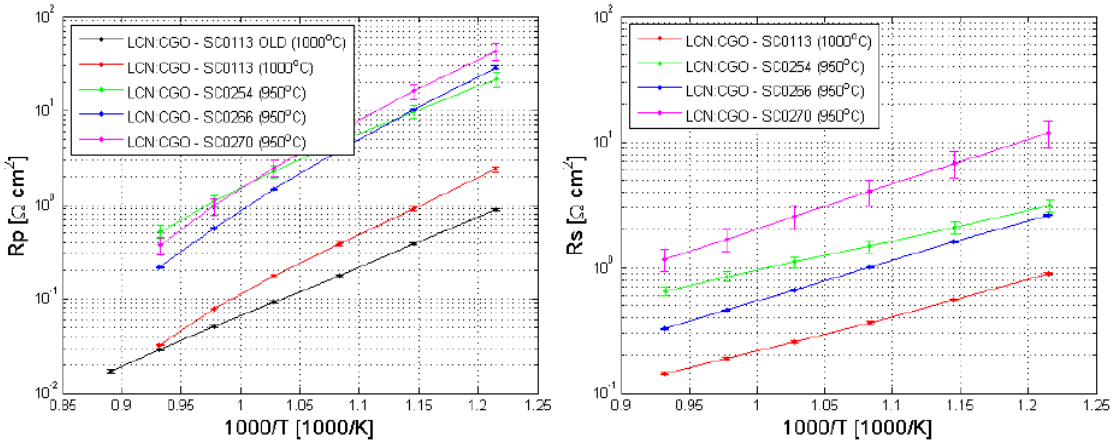


Figure 15. a) Polarisation resistance obtained in symmetric cell tests plotted in an Arrhenius plot. b) Series resistance obtained in symmetric cell tests plotted in an Arrhenius plot. All cells were manufactured by screen-printing of LCN-CGO composite layers on both sides of self-supported CGO electrolyte tapes.

Microstructural investigations showed a very fine microstructure with smaller particles in the new electrodes, which is expected to lead to increased performance, given sufficient connectivity within the electrode. Varying the sintering temperature between 950 °C - 1150 °C yielded only small changes in the performance of the cells, and electrical conductivity measurements on the cathode layers showed relatively high conductivity which indicates good connectivity between the LCN particles in the electrodes. Figure 15 shows measured polarisation (a) and series (b) resistances of the investigated LCN-CGO electrodes, obtained from symmetrical cell testing.

The results obtained on symmetrical cells were further corroborated by tests of the LCN-CGO composite electrodes on full cells. As other cathodes (LSC, LSC-CGO) were manufactured using the same furnaces, and organic additives in inks etc, but did not show the same kind of problems with reproducibility and performance, the work within this project on development of the LCN-CGO cathode was discontinued, as this sensitivity to processing conditions and/or impurities makes this material (most likely) unsuitable (or a lot less suitable) for a stable mass production of solid oxide fuel cells.

### *1.4.3 Work Package 2 - Single Cell Testing*

#### 1.4.3.1 Degradation Testing and Analysis - Overview

Degradation rates can be defined in several ways, and in this project we have used a number of commonly used degradation definitions. Degradation rate is usually given as a change of cell voltage or cell resistance with time. It is often given as a normalised, or relative, change with time (*e.g.* given as a change in % of initial cell voltage, per 1000 h). Relative degradation rates are operating point dependent and therefore makes it harder to compare degradation of a cell at different operating points, which is illustrated in figure 16.

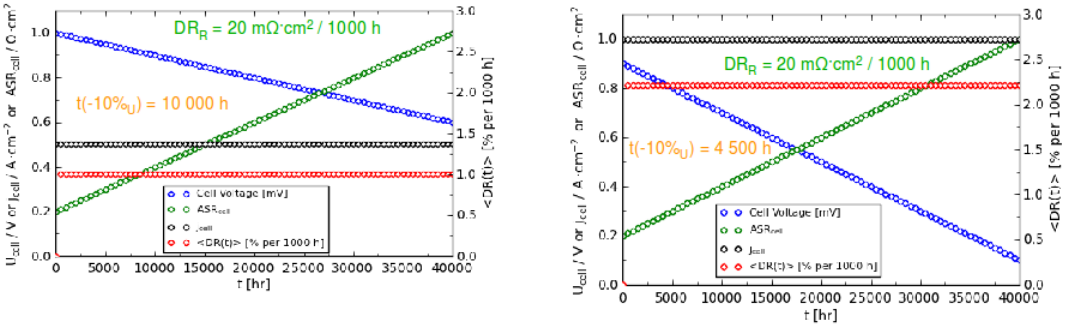


a) b)

Figure 16. a) Cell voltage calculated as a function of time for an ASR degradation rate ($DR_R$) of 20 mΩ·cm² $kh^{-1}$ at constant current (galvanostatic) operation (0.5 A·$cm^{-2}$) assuming an OCV = 1.1 V and an initial ASR = 200 mΩ·cm². If the lifetime is defined as the time when 10% of the cell voltage has been lost, then the lifetime in this case is 10 000 h. b) A calculation of cell voltage with time using the same cell and degradtion parameters as in (a) but at twice the current density (1.0 A·$cm^{-2}$). In this case lifetime would be 4500 h, although the resistance degradation is identical.

*It is desirable to use an unambiguous degradation metric, and the area specific cell resistance fulfills these criteria.* But also resistance can be assessed in different ways. For an electrochemical device one often encounters area specific secant resistance, which is defined as the cell polarisation divided by the current density (eq. 1), but also the local or tangential resistance, which in the limit of small perturbations equals the differential resistance, and is what is measured in an electrochemical impedance measurement (eq. 2). As electrochemical impedance measurements yields the differential ASR it is not directly comparable to the overall change in secant resistance, unless the polarisation curve under the test conditions is linear (which it usually isn't). However, the component or process specific information that can be obtained from impedance data is very important as it gives a good picture of the degradation contribution from the different parts of the cell, and also may yield information on the nature of the degradation.

$$ASR_{sec,corr} = \frac{\overline{OCV} - U_{cell}}{j_{cell}}$$

equation 1

$$ASR_{diff} = \frac{dU}{dj}$$

equation 2

A constant degradation rate is relatively easy to characterise when carrying out durability measurements at constant current and utilisation. Often the observed degradation rate is changing at short times and measures such as the instantaneuos degradation rate (*e.g.* d*U*/d*t* or d*ASR*/d*t*) become useful representations to visualize / quantify the changing degradation rate. In order to determine long-term degradation rate an average or linearized de-

gradation rate is often the most useful metric (*e.g.* obtained by a linear fit to the cell voltage data at longer times, where the degradation rate approaching a constant value).

As mentioned in other sections of the report, we have performed long-term durability tests of a number of advanced cells. Many of the tests were characterized by an initial more rapid loss of cell voltage which transitioned to a slower long-term degradation rate. The range of test conditions for the different durability tests was 700-800 °C and 0.5 - 0.75 A·cm$^{-2}$. As shown in Figure 17, by approximately 1500 h of cell operation, the degradation rates all converge to a similar value (<10 mV per 1000 h ; <1.5% based on cell votage, or < 20 mΩ·cm$^2$ kh$^{-1}$), nearly independent of the test conditions. Thus, for cells with LSC and LSCF based oxygen electrodes tested at 700 - 800 °C at current densities in the range 0.5 - 0.75 A·cm$^{-2}$ a test period of 1500 h was not sufficient for accurate determination of long-term degradation. The exact value is difficult to determine from only cell voltage data, it is not component specific, and illustrates the need for longer test times and/or using the advanced data analysis techniques described in section 1.4.3.2. A limited number of durability tests in the project were carried out to times exceeding 1500 h as described in section 1.4.3.4.

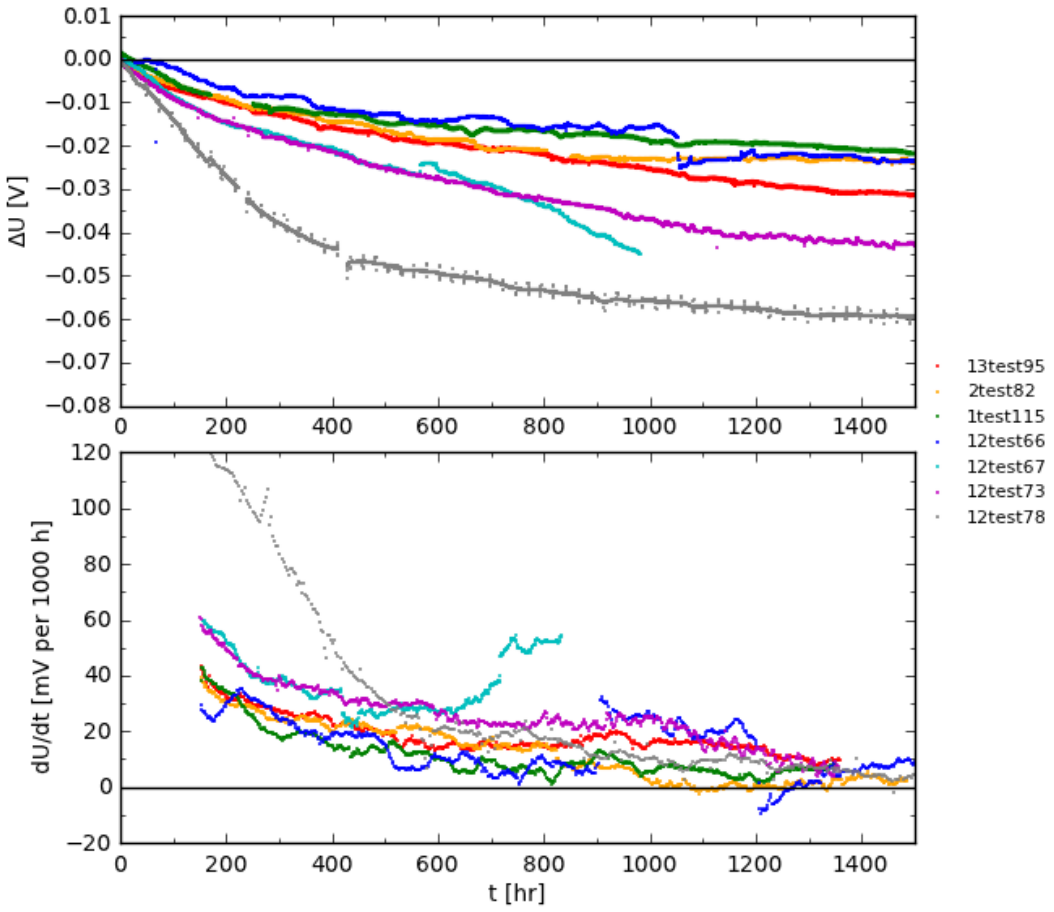


Figure 17. Change of cell voltage with time during a number of cell durability tests run on different cells at 700-800 °C and 0.5 - 0.75 A·cm$^{-2}$. The upper plot shows the time evolution of the relative voltage change (versus the initial voltage during the durability test) and the lower plot shows the time evolution of the degradation rate (derivative of the data in the upper plot, after filtering). The total operating time represented by these experiments is over 10000 h in total.

### 1.4.3.2 Detailed Electrochemical Characterisation of Solid Oxide (Fuel) Cells

We have performed DC (current-voltage curves) and AC (impedance measurements)

characterization of a number of 2.5G cells produced at Risø DTU and at TOFC, which are comprised of a porous Ni/YSZ composite fuel-electrode, dense YSZ electrolyte, dense CGO barrier layer, and porous LSCF/CGO composite oxygen-electrode. Both DC and AC measurements are used together to describe the cell performance and to diagnose set-up related issues including gas leaks and quality of contact for current collection. Impedance spectroscopy is especially useful and powerful to resolve individual resistance contributions of the cell components (each electrode and the electrolyte separately). We have applied our previously developed impedance data analysis methods to this type of cell to obtain an impedance model from which we can extract parameters (including resistance) about the cell components during operation. In addition, we have implemented new impedance analysis methods that enable us to resolve the individual resistive processes more clearly, and to connect DC and AC measurements. Besides validating the two types of measurements against each other, connecting DC and AC measurements also allows one to monitor whether the cell is in a safe operating regime, *e.g.* whether the Ni electrode is polarized too far and can form NiO, which is very useful in studying cell stability and long-term degradation.

The new and old analysis methods have both been implemented in a new data analysis software developed mainly within this project. With this software we are able to do data validation, visualize the data in the clearest way, and define models and fit the data to the models in a variety of ways, all in a very fast and systematic framework. Some of the modeling capabilities are not present in existing commercial software. This enables our research group to be at the "cutting edge" in terms of data analysis capabilities (both for impedance data and other types of data we collect).

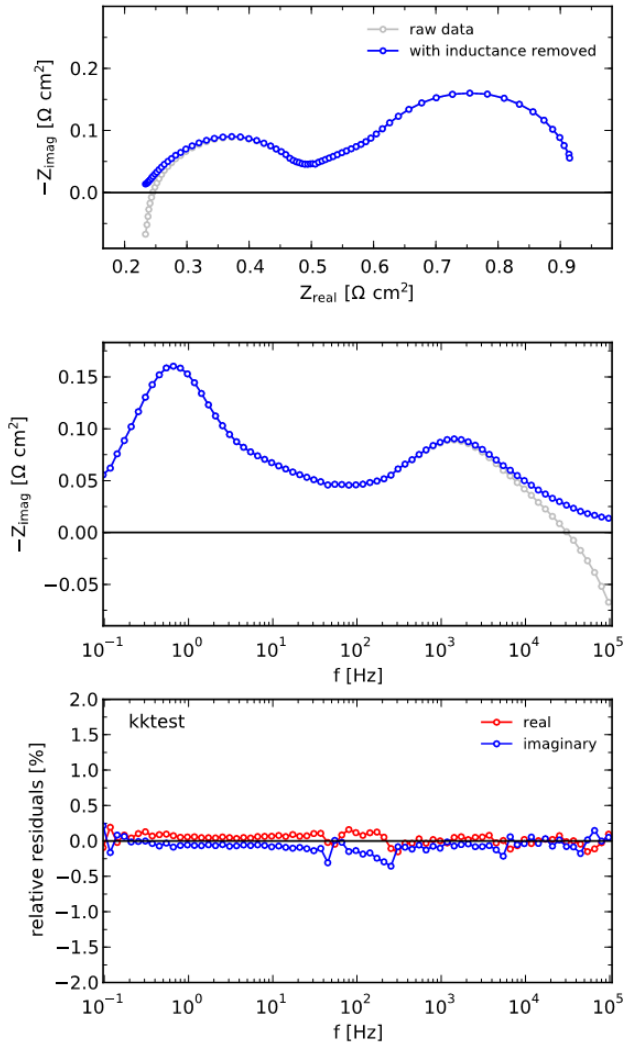


Figure 18. A typical impedance spectrum measured on a 2.5G cell at OCV at 700 °C, $H_2/H_2O$=89/11 supplied to the fuel electrode at 5.6 L/h, and air supplied to the oxygen electrode at 40 L/h. The top graph is a Nyquist (complex plane) representation of the data, the middle graph is a Bode plot of the imaginary impedance component vs perturbation frequency, and the bottom graph is showing the relative residuals obtained from a linearized Kramers-Kronig test.

A typical impedance spectrum measured at zero DC bias (at open circuit voltage; OCV) of a 2.5G cell is shown in Figure 18. Also shown in the figure is the impedance spectrum with the inductance of the wiring of the test set-up removed. The set-up response must be removed to obtain only the cell response when using advanced analysis methods. Also shown in the lower part of the figure is an assessment of the data quality using a linear Kramers-Kronig transform; the very low residuals indicate very low noise or artifacts in the data.

By systematically varying operating parameters (temperature, gas composition, and DC bias), the different responses of different parts of the cell can be observed in the impedance data due to the different relaxation times of the processes. The impedance measured on the same 2.5G cell with varying DC bias is shown in Figure 19. From Figure 19b, 5 distinct processes can be clearly identified. By varying the other operating parameters and observing the independent responses of these processes (for example, changing the fuel gas composition while keeping the oxygen-electrode gas composition fixed changes only the processes at the fuel-electrode), we have identified the processes as belonging to the Ni-YSZ fuel-electrode (processes 1 and 2), LSCF-CGO oxygen-electrode (process 4), gas diffusion (process 3), and gas conversion (process 5). The final resistance contribution is the ohmic resistance

which can be observed as the frequency intercept (towards the left) in Figure 19a. From this pre-identification process, we define a model to represent the cell and fit the model to the data, obtaining a high quality estimate of the resistance (and capacitance) contributions of each process.

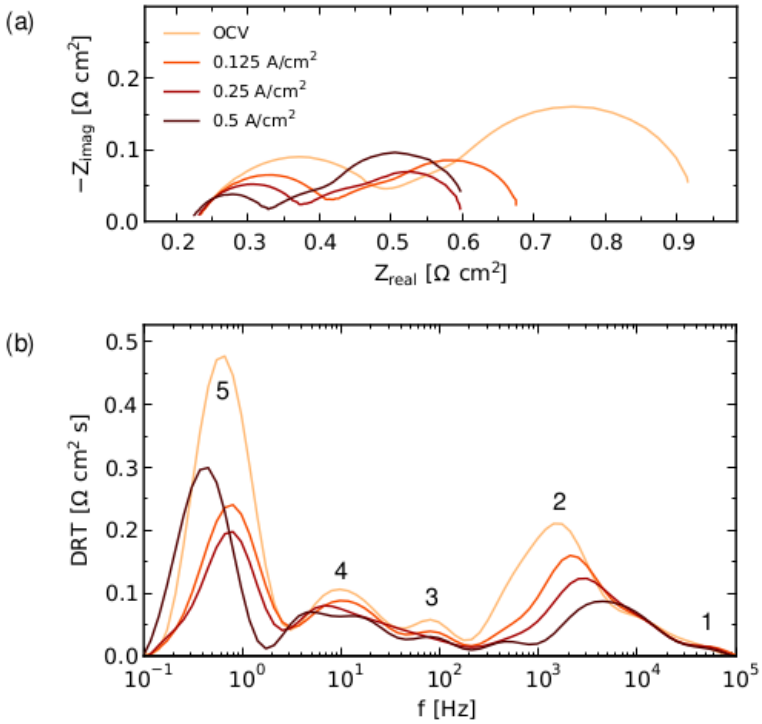


Figure 19. Four impedance spectra measured at different applied fuel cell current densities from zero (OCV) to 0.5 A/cm2. (a) Nyquist plot, and (b) distribution of relaxation times (DRT) plot from which 5 processes can be identified

First, an equivalent circuit model was developed to represent the cell and found to be a suitable representation. However, we have also taken this a step further by replacing the conventional equivalent circuit model with a "more direct" model comprised of physical-chemical equations based on electrochemistry and gas transport. *Besides being a more realistic model, the new model promises to be more useful in practical ways – it can improve the quality of data analysis and diagnosis of degradation mechanisms because fewer parameters need to be fit and the parameters that do need to be fit are physically meaningful rather than representative of the system.* For example, the low-frequency gas transport responses in the impedance data are now modeled with the parameters: the gas diffusion coefficient, dimensions of the gas flow channel (height, width, length), tortuous diffusion length through the electrode, gas composition, gas flow rate, and temperature; rather than a representative parallel resistor-capacitor type circuit for which there is no physical description of how the parameters are expected to vary with test conditions. A description of the two models and results of fitting them both to the same data are shown in figure 20 and figure 21. It should be noted that these models and the methodology are directly applicable to other cell types including more advanced cells with LSC-based oxygen electrodes (SOFC cathodes), and we have applied them to such cells in the project.

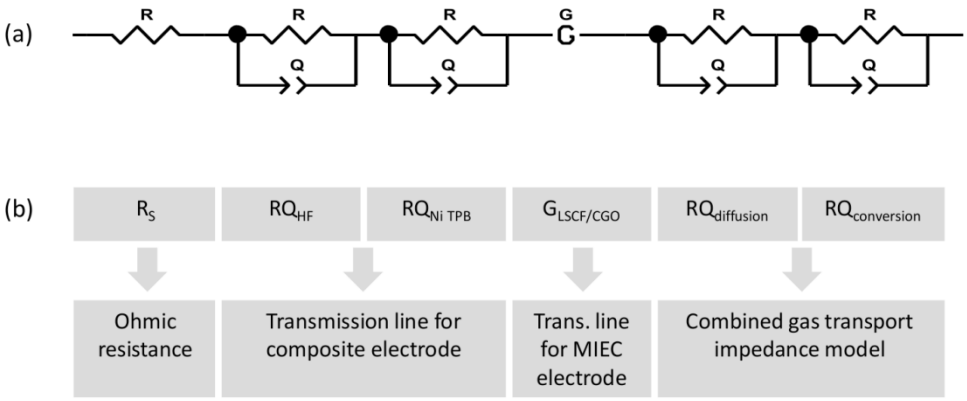


Figure 20. Impedance models developed for 2.5G cells. (a) Conventional equivalent circuit model, (b) Illustration of how we have replaced the equivalent circuit model with a model built of physical-chemical equations.

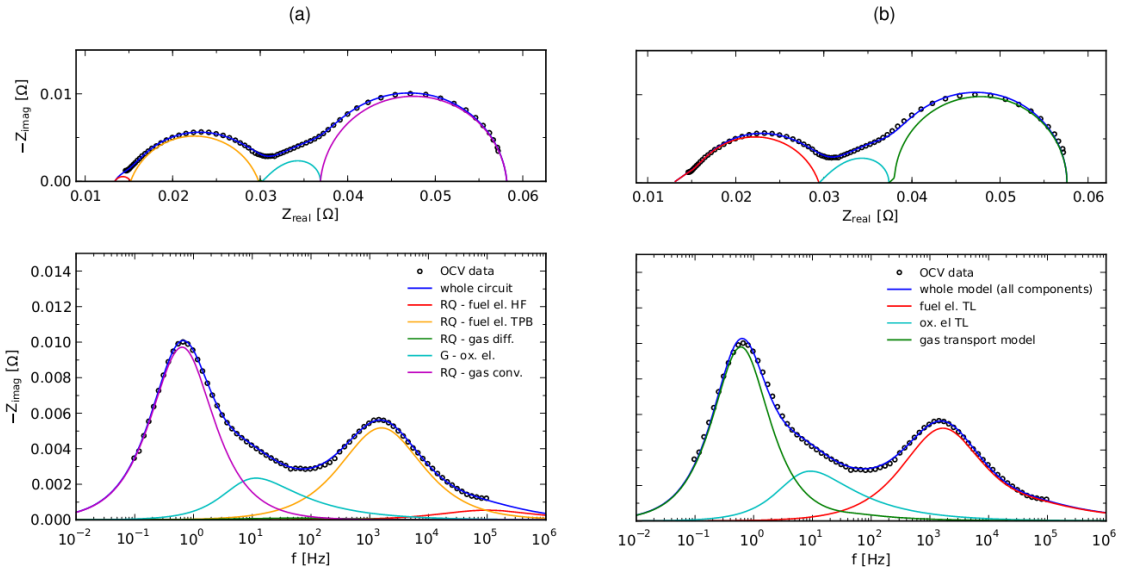


Figure 21. Results of fitting the impedance data shown in Figure 19 using the two models shown in figure 20.

In addition to using this model to diagnose degradation mechanisms during long-term testing (see M2.1.5 and section 1.4.3.3), we have also applied it to calculate overpotentials during cell polarization (Figure 22). As shown in the figure, the DC i-V curve measured separately from the impedance data measured at various current densities agrees well, validating the technique. This is a new analysis method which, among other uses, allows us to determine if the cell components are in safe operating regimes. For example, see the lines in figure 22 (bottom graph) for an estimate of how far in applied overpotential the Ni electrode is from the thermodynamic Ni→NiO transition. Crossing that threshold would severely degrade the cell, and represents a form of avoidable (extrinsic) degradation.

Without modeling the cell properly and using this analysis method, it is not possible to estimate such per-component overpotentials without using a reference electrode, which is not possible in these high-performance thin-electrolyte fuel cells (it is only possible in simpler cell geometries used for non-application-oriented scientific studies).

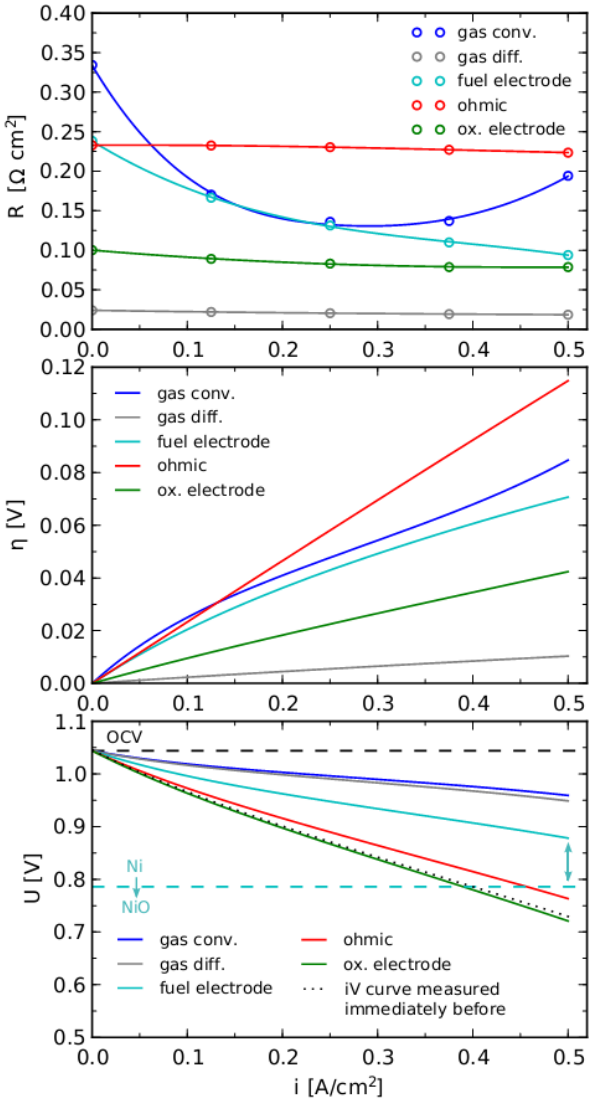


Figure 22. The resistance contributions of the 2.5G cell [*i.e.* LSCF-CGO composite cathode / CGO barrier layer / YSZ electrolyte / Ni-YSZ anode / Ni-YSZ support] at various applied current densities, obtained from the impedance measurements and fitting process described above, as the cell is ramped up in current to start a durability test. The resistance obtained from the impedance measurements are local/instantaneous current-voltage slopes and are integrated to obtain the overpotentials, which are then subtracted from the open-circuit voltage to obtain the absolute potential at each component of the cell.

### 1.4.3.3 Degradation Analysis of Cells with LSCF-based Cathodes

A number of degradation tests on 2.5 G cells with LSCF-CGO cathodes were carried out in the project with the aim of quantifying the degradation rate of each component/process in the cell, and to learn more about factors controlling the degradation of the cells. The 2.5G cell described in section 1.4.3.2 was operated for a long-term durability test. The evolution of the cell voltage at 0.5 $A \cdot cm^{-2}$ at 700 °C in humidified $H_2$ is shown in Figure 23. The voltage degradation rate becomes lower throughout the test and approaches a value below 10 mV per 1000 h, corresponding to < 20 $m\Omega \cdot cm^2\, kh^{-1}$, within an aging period of 1500 h. However, from only the cell voltage curve, it is not known which cell component is degrading. Furthermore, estimating the long-term degradation rate is difficult due to measurement noise, and that the degradation rate is changing (decreasing) throughout the test.

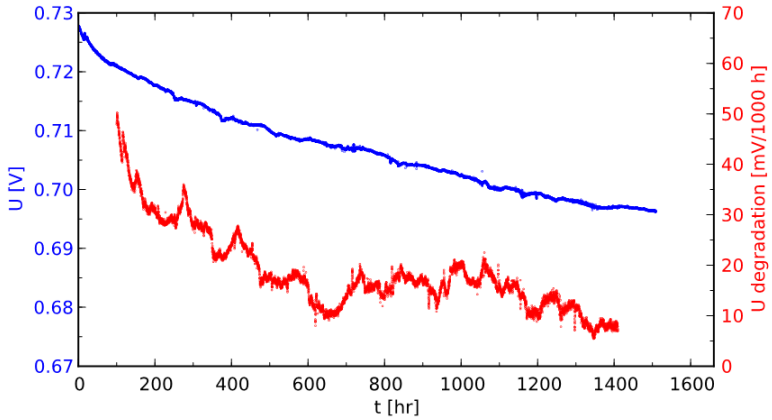


Figure 23. Durability test of the same 2.5G cell as used to exemplify the strategy and methodolgy used for detailed analysis of performance data (see section 1.4.3.2). The voltage degradation corresponds to the instantaneous (dU/dt) degradation rate.

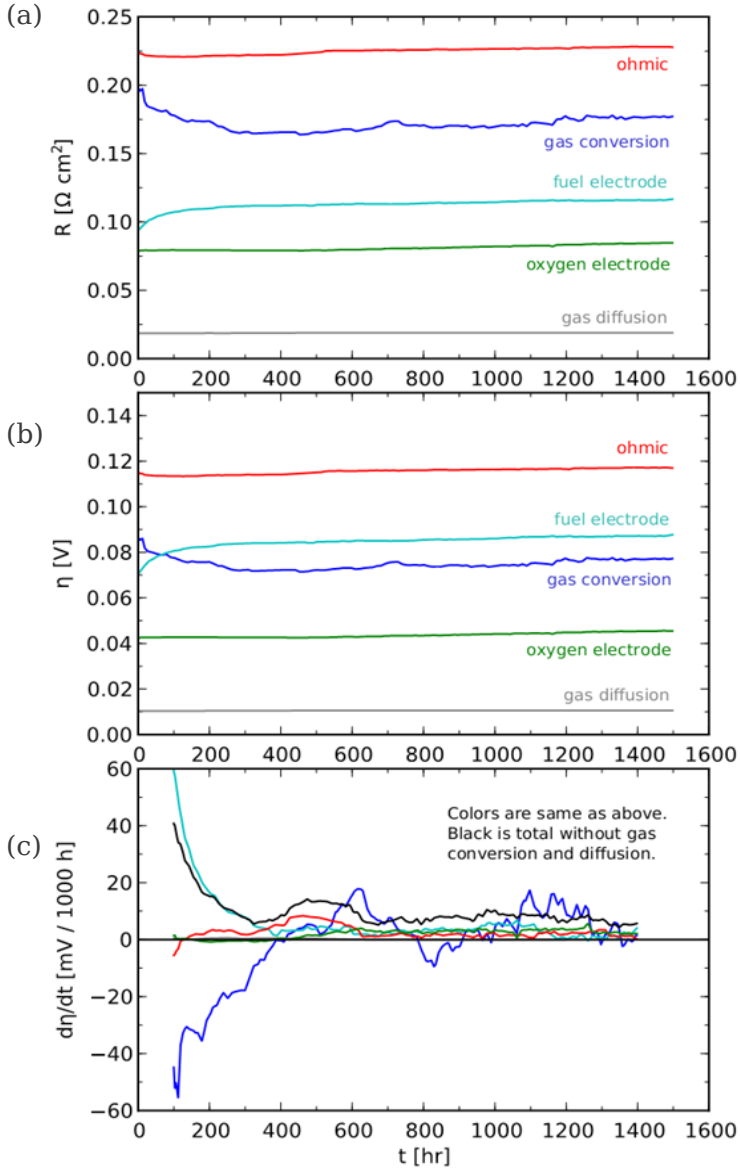


Figure 24. Breakdown of (a) cell resistance contributions, (b) overpotentials, and (c) degradation rates of overpotentials (200 h moving average), versus time during the long-term durability test shown in Figure 23. The polarisation resistance of the LSCF-CGO cathode is 75-80 mΩ·cm$^2$ initially.

This method of breaking down the resistance and calculating overpotentials described above was applied to this durability test, by analyzing and fitting all of the impedance data measured during the 1500 h test (Figure 23). The overpotential of each resistance contribution was calculated and plotted versus time (Figure 24 b). For the overpotential versus time calculation, it was assumed that the resistance increase for each component resulted from a phenomenon that would cause the overpotential change to be directly proportional to the resistance change, like loss of active area or active reaction sites. From this analysis, we find that the long-term degradation (after initial more rapid transients) of the total cell overpotential not including gas concentration processes (gas conversion and diffusion) is approx. 7 mV per 1000 h, corresponding to 14 $m\Omega \cdot cm^2\, kh^{-1}$. The corresponding rates of each component are 3.2, 1.4 and 2.7 mV per 1000 h for the Ni/YSZ fuel-electrode, the ohmic voltage drop (mainly the electrolyte), and the LSCF-CGO oxygen-electrode respectively (see figure 24 c, and the same results were obtained by linear fits of the overpotential profiles of Figure 24 b for the last 900 h of the test). Another useful outcome of this type of analysis is that by isolating the gas conversion resistance, it became clear that the noise in the cell voltage curve was due to variations in the gas conversion resistance, which correspond to small changes in the gas supply (flow rate / composition). The long term degradation rate of the remaining resistance contributions corresponds to that of the cell itself, and could be determined with lower noise (see the black line in Figure 24 c).

#### 1.4.3.4 Degradation Analysis of Cells with LSC-based Cathodes

The two milestones M2.1.3 "Degradation rate of less than 1% per 1000 h obtained in a 1500 h long-term test at 0.75 A $cm^{-2}$" and M.2.1.4 "Detailed electrochemical characterisation of a cell with an alternative cathode completed" were defined and the work presented in this section is part of the work carried out towards fulfilling these project milestones. A significant effort was placed within WP1 on development of LSC-based cathodes as an alternative to the LSM, and LSCF, based cathodes already in use. LSC-based cathodes have been shown to yield very low polarisation resistances but the long-term stability of such cathodes has not been explored in great detail. As discussed in section 1.4.3.2 a good model for the cell is essential in order to analyze the degradation in a component or process specific way, as this is what allows an accurate breakdown of the losses into constituent contributions. Electrochemical characterisation of the cell at selected conditions (various gas compositions, current loads, and temperatures) is necessary in order to assign the observed resistance contributions to specific processes taking place in the cell. The same methodology was applied in this work as outlined in section 1.4.3.2.

Available published electrochemical data on LSC cathodes measured on symmetrical cells at has shown that the degradation rate of LSC at open circuit voltage (OCV) is relatively high.[6] There are also literature reports on the degradation of the related mixed electronically and ionically conducting (MIEC) perovskite material, $La_{0.58}Sr_{0.4}Co_{0.2}Fe_{0.8}O_{3-\delta}$ (LSCF) applied onto anode supported cells (ASC) that show substantial cathode degradation at OCV, which increases with lower operating temperatures.[7] The results obtained in this project, and results reported by others, have shown that cells with LSCF-based cathodes are relatively stable when operated in the temperature range 700 - 800 °C (with cell voltage degradation rates in the order of 1% / 1000 h).[8] The degradation of LSCF has also been tied to loss of Sr from the LSCF.[9] The Sr activity of LSC is greater than for LSCF which potentially could lead to a faster loss of performance than that observed for LSCF.

---

6 P. Hjalmarsson, M. Søgaard, and M. Mogensen, Solid State Ionics, 179, 1422–1426 (2008).

7 Endler-Schuck C, Leonide A, Weber A, Uhlenbruck S, Tietz F, Ivers-Tiffée E (2011) J Power Sources 196:7257-7262

8 A. Mai, V. A. . Haanappel, S. Uhlenbruck, F. Tietz, and D. Stöver, Solid State Ionics, 176, 1341–1350 (2005).

9 F. Tietz, A. Mai, and D. Stöver, Solid State Ionics, 179, 1509–1515 (2008).

From a technological point of view, it is important to determine the degradation of a SOFC under current load rather than at OCV as the cell is expected to be operated with a power output during most of its life time. There are some indications in literature that cells with LSC-based cathodes yield quite stable performance when operated under current (0.22 - 0.5 $A \cdot cm^{-2}$) at temperatures as low as 650 °C.[10,11]

Two types of cells with LSC-based cathodes were tested at two different current loads in the project. The test periods were 2000 - 3200 h under current load. The key cell parameters are listed in table IV.

Table IV: Key Cell Parameters

| Cell Type | Cathode | Barrier | Electrolyte | Anode |
|---|---|---|---|---|
| A | LSC | CGO, screen-printed | YSZ | Ni-YSZ |
| B | LSC-CGO | CGO, PVD | YSZ | Ni-YSZ |

Figure 25 shows polarisation curves of the two cells obtained at 700 °C, before durability testing. The polarisation resistance of the two cells was very similar, and the difference in cell performance is explained mainly by a greater ohmic resistance (manily due to electrolyte + barrier layers) for cell A, which had a screen-printed barrier layer. The fuel utilisation corrected resistance calculated from the polarization curves was 0.26 $\Omega \cdot cm^2$ for Cell A and 0.15 $\Omega \cdot cm^2$ for Cell B. The target ASR for a repeating unit (cell + interconnects) in a SOFC stack is defined as 0.22 $\Omega \cdot cm^2$ (2015 target) and 0.18 $\Omega \cdot cm^2$ (2020 target) in the national roadmap for SOFC implementation, which makes this cell type an interesting candidate to achieve these goals.

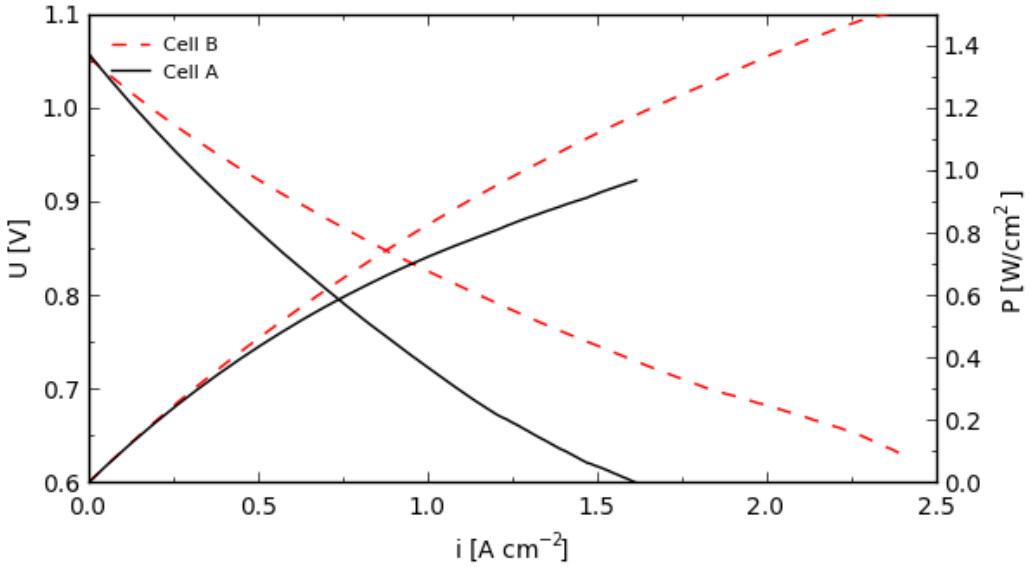


Figure 25. Polarization and power curves for Cell A and Cell B measured at 700 °C, with a fuel composition of 80% $H_2$ + 20% $H_2O$, and air (compressed air or a mixture of $N_2$ + $O_2$) fed to the cathode.

[10] Steinberger-Wilckens R, Buchkremer HP, Malzbender J, Blum L, de Haart LGJ and Pap M.; 9th European Solid Oxide Fuel Cell Forum, Lucerne (CH). 2010;2–31.

[11] Christiansen N, Holm-Larsen H, Jørgensen MJ, Wang CH, Ramousse S and Hagen A.; 9th European Fuel Cell Forum; 2010: 2:80–89.

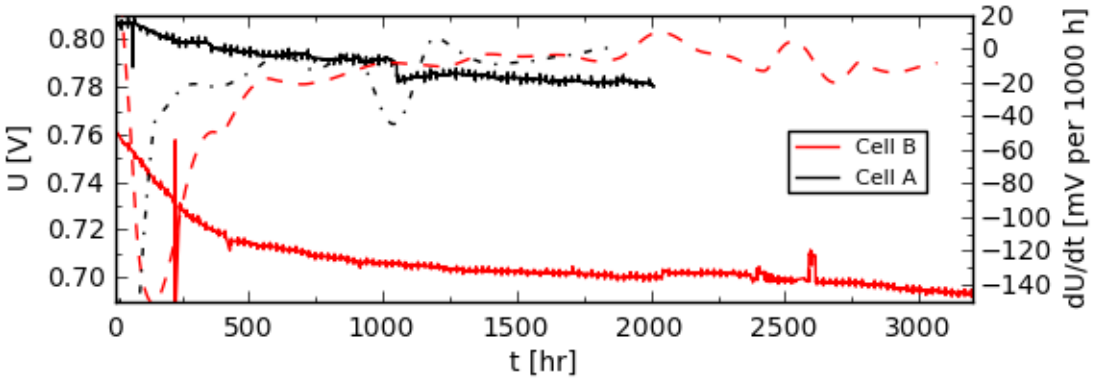


Figure 26. Galvanostatic cell voltage curves measured at 0.5 A·cm$^{-2}$ (cell A) and 0.75 A·cm$^{-2}$ (cell A) at 700 °C, with a humidified $H_2$ as fuel, and air (compressed air or a mixture of $N_2$ + $O_2$) as oxidant. Both cells were operated at a fuel utilization of ~60% and an oxygen utilisation of ~20%. The dotted lines shows the instantaneous voltage degradation rate (dU/dt).

Figure 26 shows the cell voltage as a function of time when a cell of type A and a cell of type B were operated galvanostatically (at constant current) at a current density of 0.5 and 0.75 A·cm$^{-2}$, respectively. The total voltage loss over the last 2200 h in the test of cell B amounts to 13.9 mV, which corresponds to 6.3 mV per 1000 h or 8.4 mΩ·cm$^2$ kh$^{-1}$. The relative degradation rate (based on the cell voltage) was thus approximately 0.9% per 1000 h. This long-term degradation rate is close to that obtained in 6test41, which was a test of a cell with an LSC-CGO cathode and a half-cell with a CGO-ScYSZ bilayer electrolyte and a Ni-ScYSZ anode, reported in section 1.4.2.1.

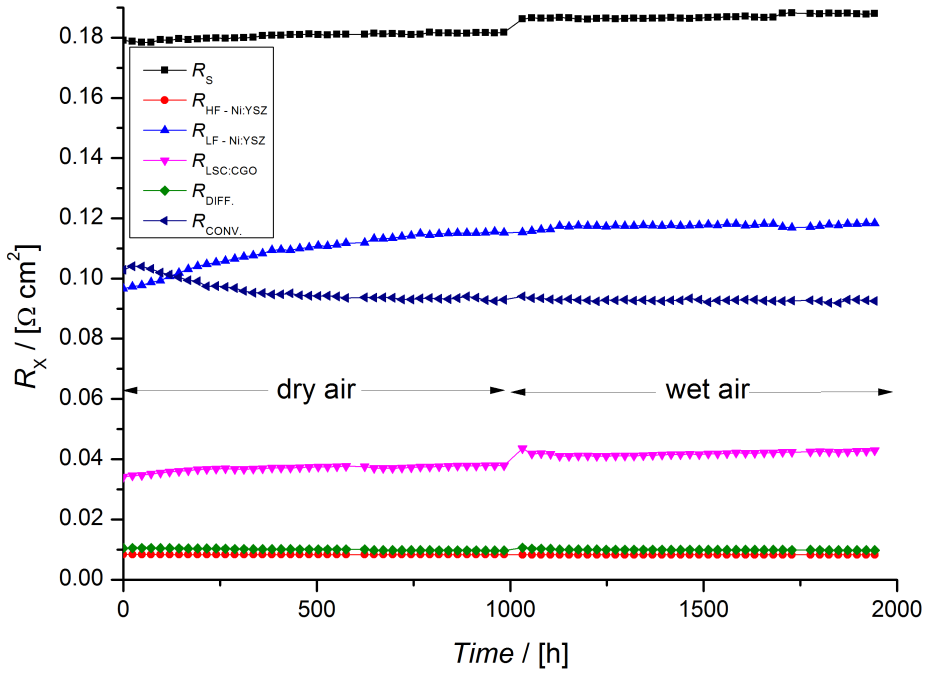


Figure 27. Evolution of the process specific resistances elements during the galvanostatic test of Cell A. The resistance $R_{LSC-CGO}$ is mislabeled in the figure, it corresponds to $R_{LSC}$. The small jump in series and cathode resistance at t ~ 1000 h was caused by an accidental interruption of the oxidant gas flow which led to a short period oxygen starvation at the cathode. Note that the cathode polarisation resistance is about 34 mΩ·cm$^2$ at the start of the test, which can be compared with ~ 104 mΩ·cm$^2$ for the anode.

However, the degradation rate in 6test41 was determined from data in the first 1000 h of the test (the test duration was only 1000 h), and further testing should be carried out to longer test times, to verify this low apparent degradation rate.

Component specific degradation analysis was carried out using a model corresponding to the equivalent circuit developed in section 1.4.3.2 (figure 20a) and is shown for cell A in figure 27. The process specific long-term degradation rates obtained for cell A and B from deconvolution of the impedance data collected during the durability tests last are summarised in table V.

The total long-term degradation rate determined from the impedance data is ~6-7 $m\Omega \cdot cm^2\ kh^{-1}$ for cells A and B (see table V), which correlates well with the long-term ($\Delta ASR_{secant}$) degradation rate found from cell voltage data (8.4 $m\Omega \cdot cm^2\ kh^{-1}$).

Table V: Degradation rates obtained from EIS data measured during operation. All long-term degradation rates represent linear approximations of the degradation rate during the last 1000 h (Cell A) - 2000 h (Cell B) of testing.

| Cell Type | Cathode | Barrier | $R_{series}$ / $m\Omega \cdot cm^2\ kh^{-1}$ | $R_{HF,Ni-YSZ}$ / $m\Omega \cdot cm^2\ kh^{-1}$ | $R_{LF,Ni-YSZ}$ / $m\Omega \cdot cm^2\ kh^{-1}$ | $R_{cathode}$ / $m\Omega \cdot cm^2\ kh^{-1}$ | $R_{diffusion}$ / $m\Omega \cdot cm^2\ kh^{-1}$ |
|---|---|---|---|---|---|---|---|
| A | LSC | CGO, screen-printed | ~2 | ~0 | ~1-2 | ~2 | ~0 |
| B | LSC-CGO | CGO, PVD | ~3 | ~0 | ~3 | ~1 | ~0 |

The overall degradation includes the rapid and greater in magnitude initial degradation of the cells and was determined from the secant resistance (see section 1.4.3.1 for definitions) calculated from dc polarisation measurements before and after the galvanostatic durability test, and from the initial and final cell voltage assuming that the OCV was constant during the test. The $\Delta ASR_{secant}$ was found to be 26 (27) and 33 (27) $m\Omega \cdot cm^2\ kh^{-1}$ for cell A and B (values in brackets are calculated from inital and final cell cell voltage during operation), while the total change in the local slope, the tangential ASR ($\Delta ASR_{tan}$), at the operating point (0.5 A $cm^{-2}$ or 0.75 A $cm^{-2}$) was determined to 12 (14) and 13 (14) $m\Omega \cdot cm^2\ kh^{-1}$ for cell A and B (values in brackets are the total change in $ASR_{tan}$ based on EIS data).

The stability of the LSC cathode (cell A) to moderate amounts of water vapour in the oxidant feed gas was tested by humidification of the gas for 1000 h (from t = 1000 h to the end of the test) to yield an average volumetric steam content of about 4.5%. No significant change in the cathode degradation rate was observed during this latter 1000 h period, indicating that the water tolerance of LSC-based cathodes is excellent under these conditions.

### 1.4.3.5 Performance and Stability of Cells with Nano-Structured Cathodes

The milestone M.1.2.2 "Two cells with different nanostructured cathodes developed and delivered for testing" were defined for WP1. The work related to this milestone is reported here. Two systems were investigated, both using a platform consisting of a half-cell with the components Ni-YSZ support / Ni-ScYSZ anode / ScYSZ electrolyte / CGO barrier layer / Porous CGO backbone, with the latter used as an ionically conducting scaffolding into which the electrocatalyst material was infiltrated using metal nitrate precursor solutions.

The first system, an infiltrated LSC cathode, was developed in a PhD project carried out by A. Samson ("Cathodes for Solid Oxide Fuel Cells Operating at Low Temperatures", 2012). This kind of electrode has been shown to yield very high performance, with a low polarisation resistance as low as 44 $m\Omega \cdot cm^2$ at 600 °C. The polarisation resistance of this this nanostructured cathode was shown to increase during aging at 600 °C and at zero bias (OCV) and levels off at about 70 $m\Omega \cdot cm^2$ after 450 h. This electrode was integrated on the platform described

above and its' performance and durability was tested in this project at 700 °C and at a current load of 0.5 A·cm$^{-2}$.

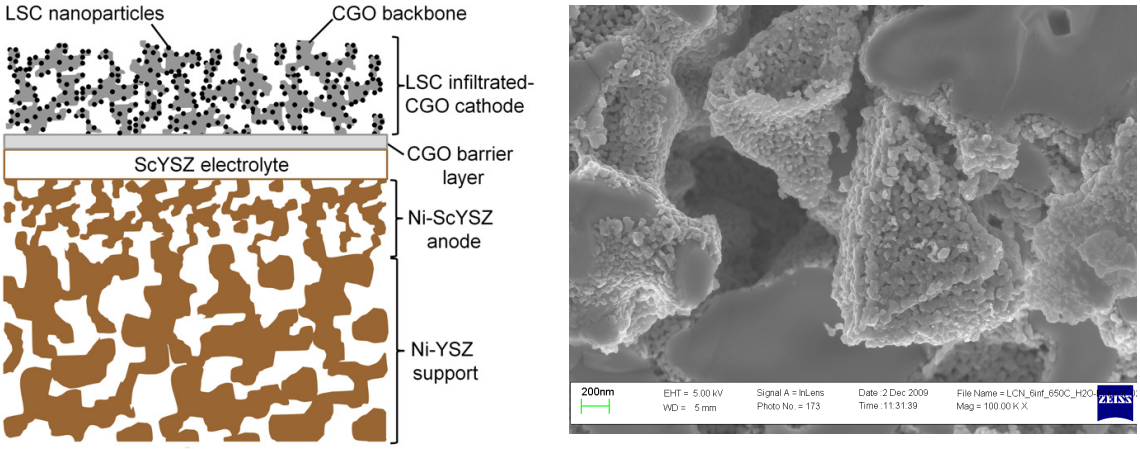


Figure 28. (a) Schematic of the anode-supported cell used in this study (b) Micrograph of LCN infiltrated into a LCN-CGO backbone on a symmetric cell

The second system investigated was an infiltrated $LaCo_{1-x}Ni_xO_{3-\delta}$ (LCN) cathode. Figure 28a shows a schematic of the cell and figure 28b shows a micrograph of the infiltrated LCN particles inside a porous LCN-CGO backbone. Electrochemical studies of these cathode layers in a symmetric cell configuration have shown very low electrode polarization resistances ($R_p$) of 45 mΩ·cm$^2$ at 650°C, but still substantially higher than that observed for the infiltrated LSC electrodes, which yields 44 mΩ·cm$^2$ at 600 °C. In this study LCN was infiltrated into a pure CGO backbone, identical to that used for LSC infiltration.

Figure 29 shows polarisation curves obtained at 750 °C for two nominally identical half-cells, one infiltrated with LSC, and the other with LCN. The significantly lower performance of the LCN infiltrated cells is due to a large difference in series resistance (confirmed by impedance measurements). The reason for this difference is not known at project completion, but by further optimization it is expected that the LCN infiltrated cathode would yield a performance significantly closer to that of the LSC infiltrated cell. The polarisation resistance measured of the two cells was very similar at 750 °C indicating a negligible (or at least similar) cathode resistance contribution at this temperature.

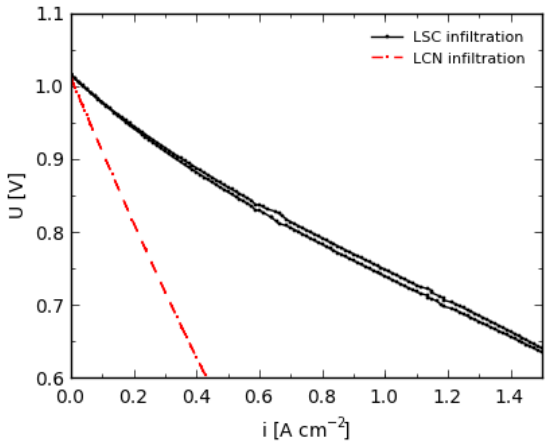


Figure 29. Polarisation curves recorded for the LCN and LSC infiltrated cells at 750 °C, with a fuel composition of 80% $H_2$ + 20% $H_2O$ and air fed to the cathode.

The cell voltage history plot of the long-term durability test of the LSC infiltrated cell is displayed in figure 30 and figure 31 shows the impedance spectra recorded during operation for 1500 h at 700 °C and at 0.5 A·cm$^{-2}$.

The two nanostructured cathodes manufactured and tested here on full cells yield good performance, and the durability test of the nano-LSC cathode showed excellent stability. This is the first test of such a cathode under industrially relevant operating conditions (0.5 A·cm$^{-2}$, 700 °C and 20 % oxygen utilization), and no significant degradation could be detected during 1500 h of operation. However, after switching off the current and leaving the cell idle for a period of time a significant performance decrease was observed, which opens up questions about possible activation/passivation processes in such cathodes, and the reversibility of these processes. This is important to explore further in order to understand the technological potential of these cathodes.

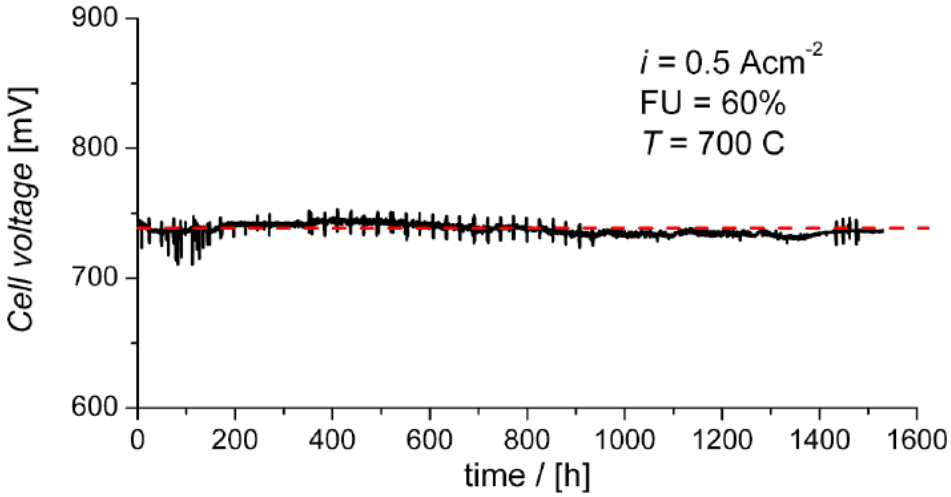


Figure 30. Cell voltage history plot from the galvanostatic durability test carried out at 700 ºC, 0.5 A·cm$^{-2}$, 60% fuel utilization, and 20% oxygen utilization. The red dashed line represents the initial voltage under operation and is only a guide to the eye.

The net loss of cell voltage during the galvanostatic durability test was close to 0 mV, but considering the variations in the observed cell voltage longer test times would be needed to distinguish the actual degradation rate. However, it is clear that it is a small degradation, and this both further supports other observations of the excellent stability of the Ni-ScYSZ anode, and points to acceptable stability also of an infiltrated nano-structured cathode (LSC).

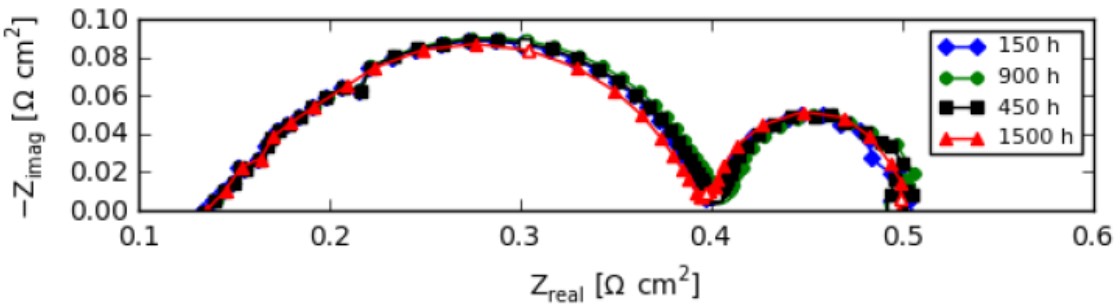


Figure 31. Nyquist plots of the impedance data recorded during the galvanostatic durability test of the anode-supported cell with a nano-LSC .

The infiltrated electrodes represent an interesting system also from a manufacturing point of view, and future efforts should also investigate the potential for simplified and cheaper production using this type of electrode.

### 1.4.3.6 Long-Term Stability of the Mechanical Properties of Anode-Supported SOFCs

Only limited information is available about the evolution of the mechanical properties of SOFCs during long-term operation, and this topic was addressed in this project using a custom built test rig that is capable of measuring the mechanical properties of the cells in (dilute) fuel gas and at operating temperature. As most of the strength of a cell is due to the zirconia based half-cell, i.e. Ni-YSZ support/Ni-YSZ anode/YSZ electrolyte, the effort focussed on the mechanical properties of such half-cells. To study the strength characteristics of the ceramic fuel cells, Weibull statistics were employed on the fracture data, which was obtained using four-point bend tests. By determining the Weibull strength and Weibull modulus, the trends in strength and reliability of the samples at the specific temperature and time intervals over can be determined. However, to obtain useful results at least 30 samples per testing condition must be used. This presented a problem in that a high volume of samples needed to be aged over the lifetime of the project. To solve this problem a sample holder was designed that would allow up to 350+ samples to be safely loaded and undergo the aging process (figure 32).

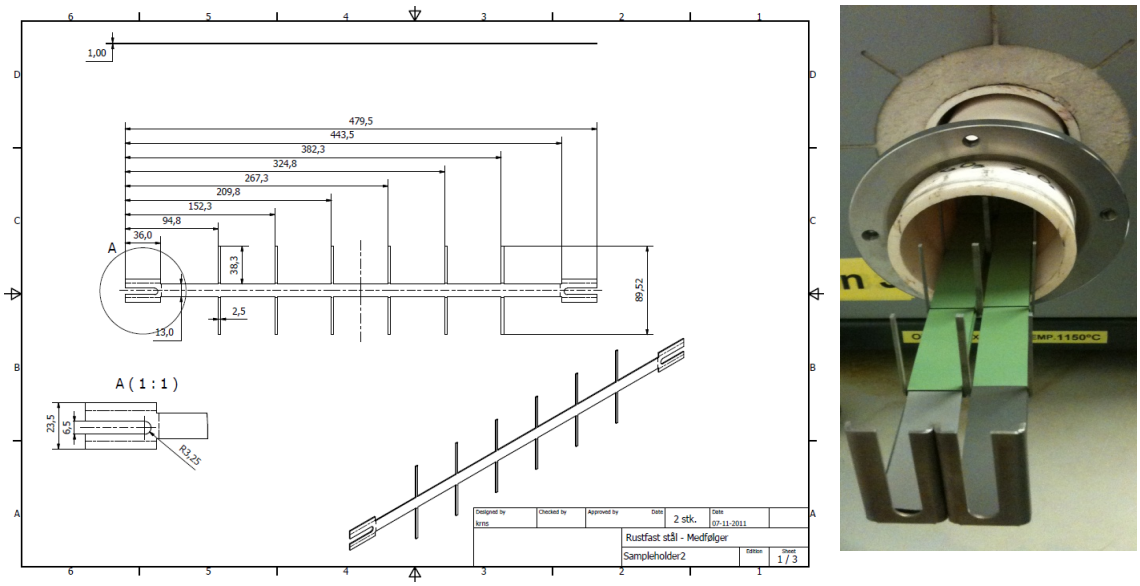


Figure 32. Design of the sample holder (left) and the samples being introduced into the cylindrical furnace (right).

The samples were aged in a tube furnace in reducing atmosphere simulating stack conditions expected at the outlet (high ratio of water to hydrogen) at a temperature of 800 °C.
The samples aged for 500 hours have a Weibull strength of 99MPa, while the samples aged for 1000 hours and 1500 h have a Weibull strength of 102 MPa, and 105 MPa, respectively. This increase is small, but it does show a statistically derived increase in strength between the samples (figure 32). The volume fraction of porosity of these samples is very similar, and as such the porosity, at this point, is deemed to not be a factor in the change in Weibull strength.

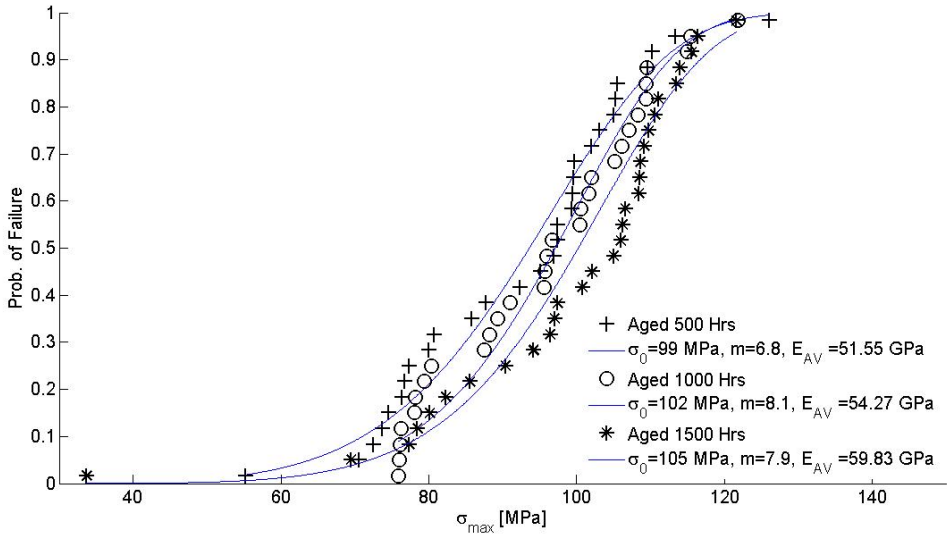


Figure 33. Weibull plot showing the probability of failure of the samples due to the maximum stress, with the Weibull strength given for samples aged 500 h, 1000 h and 1500 h. All measurements were made in reducing atmosphere at 800 °C.

The reason for this strength increase has not been fully determined. Initial investigations accounting for the creep, which is known to occur, cannot explain this increase in strength. If creep were occurring it would enhance the strength to a greater degree, by reducing residual stresses in the cells, than what is observed between batches. However, further investigation would need to be conducted to determine if another phenomena is occurring that is affecting creep; if creep is occurring in an abnormal way, or if another phenomena is solely responsible for this increasing strength trend.

Future efforts should focus on investigating the reason for this strength increase as it might be used to construct stronger cells, by determining the strength profile of cells over long periods in stack operational conditions. The study should be extended to longer durations in order to investigate the validity of these initial findings. It would also shed light on the effects of creep at longer ageing periods where, in theory, creep should detrimentally affect strength post residual stress relaxation. These results would have direct relevance to lifetime of a cell in terms of strength.

### *1.4.4 Work Package 3 - Development and Testing of Auxiliary Components*

The overall objective of WP3 was to continue the development of auxiliary components, mainly gaskets, for cell testing. The development includes characterisation with respect to material properties and gas leak rates at various temperatures. The most important parameters for designing a SOFC seal that fulfils the requirements are related to the development of a sealing material that is capable of tightness at elevated pressure (1.3 times operational pressure) and temperature (5% above the maximum foreseen temperature) as well as under chemical and electric influence both during normal and foreseen abnormal operation without any effect on the functional characteristics during the whole lifetime. For single-cell and stack testing at operating temperatures below 750 °C, three types of alternative sealant materials were considered (metal/alloy, compressive inorganic non-metallic seals, and glass). Many of the sealant (gasket) candidates were based on different coatings applied on both sides of thin steel frames. Screen-printing was used to apply the coatings on the steel frames and suitable and environmentally friendly ink vehicles were developed by IRD for this purpose.

Further development took place in this project of a previously investigated proprietary glass with a TEC of 12-13 $1x10^{-6}$ $K^{-1}$, which fits very well with other cell components (ForskEL project #2008-1-0045). The glass can be sealed at 750 °C. A rapid crystallisation into temperature stable phases after melting makes it possible to use this glass over a large temperature range from 30-970 °C, which covers the operation range of several types of fuel cells. The milled glass was processed into an ink and printed on steel frames. Theses frames were successfully testes in a stack element test for 500 h under various conditions without showing any signs of sealing related degradation. The handling and manufacturing of such steel frames is simple and less time consuming compared to state of the art sealing with glass bars. This work completed milestone "M3.2 Development of simple manufacturing route for a low-temperature glass sealant component"

An important part of the overall objective in WP3 was to evaluate the functionality of 3 different types of seals for potential use in single cell testing. Especially the gas tightness as function of the temperature was of interest (M3.1), since this data, once available, can help determine necessary sealing temperatures and whether these materials can be used as alternative sealants in cell testing. The seals in group.

An custom-built test stand designed and operated by IRD was used to measure leak rates of several different seals under operation conditions. In all cases, except from Au frames and compressive inorganic seals (Mica), the sealing materials were applied by screen printing on steel frames, which could be directly tested in the alumina test house at IRD. The following 6 materials were tested during the project:

Group I: Glass based seals
1) Standard glass
2) Low temperature glass

Group II: Metal/alloy
3) Au frames
4) Pure Ag
5) Ag + filler

Group III: Compressive seals
6) Mica

Results for Group I (glass based seals):

An overview of the obtained leak rates is given in Fig 34. The following temperature profile was used for sealing in Group I: heating with 100 K/h to 950 C, cooling down with 100 K to 600 °C. Leak rates were measured from 600 to 850 °C in 50 °C increments. The standard glass showed very low leak rates (the lowest within this project) in the temperature range from 600-900 °C. However, a significant leakage is evolved when the standard glass is cooled to room temperature probably due to TEC mismatch between the alumina test house and the glass. It is not yet known where this gasket can form tightness again upon re-heating to the seal-temperature (940ºC), but due to crystallisation in the glass this seems doubtful. Based on these results, the use of this glass in standard cell tests is recommended, but in future tests, which contain thermal cycling, alternative sealants should be used. In additional experiments the sealing temperature was decreased from 950 °C to 850 °C and 800 °C. The obtained leak rates at 750 °C are one order of magnitude higher compared to the high temperature sealing process, but still in an acceptable range.

The low temperature glass did not show good sealant properties in these tests, obtained leak rates at 600 °C were significantly higher than for the standard glass. The reason for the high leak rates is poor wetting of the glass on the surface of the alumina test house. Nevertheless, this glass showed adequate leak tightness in a stack element test carried out in the project, and future experiments in *e.g.* a steel test house (where wetting is much improved), would allow a better assessment of the leak tightness of this glass.

Results for group II (metal/alloy):
Au based gaskets sealed at 850 °C and 900 °C did not result in leak tight seal. The obtained values were too high to determine an accurate leak rate. The reasons for the failure were a) a too rough surface of the gaskets and b) too low pressure and temperature during the sealing process. Au gaskets could most likely be used to make gastight seals if a higher sealing temperature and/or more weight load were applied, but such results would not be comparable to the rest of the experiments and were therefore not performed here. Decreasing the roughness of the gold seals should also lead to significantly improved results. The following temperature profile was used for Ag based sealings in Group II: Heating with 100 K/h to 940 °C, cooling down with 50 K/h to 600 °C. Pure Ag possesses good sealant quality when sealed at 940 °C (fig x). For pure Ag a temperature dependency was found. Lower leak rates at lower temperatures were obtained, at 650 °C the leak rates were even smaller than for the standard glass. Even at room temperature the seal was gas tight, which indicates that this type of sealant may be useful in a significantly wider temperature range than is commonly true for glass-based sealants. Also for the Ag+filler sealant system very low leak rates were obtained (Fig X). In this case no significant temperature dependence was found. It has to be mentioned, that Ag based materials cannot withstand a long sealant time at 940 °C, probably because the sealant temperature is close to the melting point of pure Ag, which is 962 °C.

Result for group III (compressive seals):
Mica gaskets have been characterised for tightness in the same way as the Au gaskets. The mica gasket showed relatively poor sealant properties mainly due to the as-received rough surface that was not evened out during the test. Furthermore, the mica gasket expanded ~44% in height during the test. Lower leak rates could be obtained if the weight load was increased to 18 kg and the sealing temperature to 1050 °C (fig 34). Compared to seals in Group I and II, the leak rates are 5-7 orders of magnitude higher. Even if these value are relatively high, Mica seals could be an interesting option for the air side in cell tests or for test setups that use higher pressure due to their easy handling.

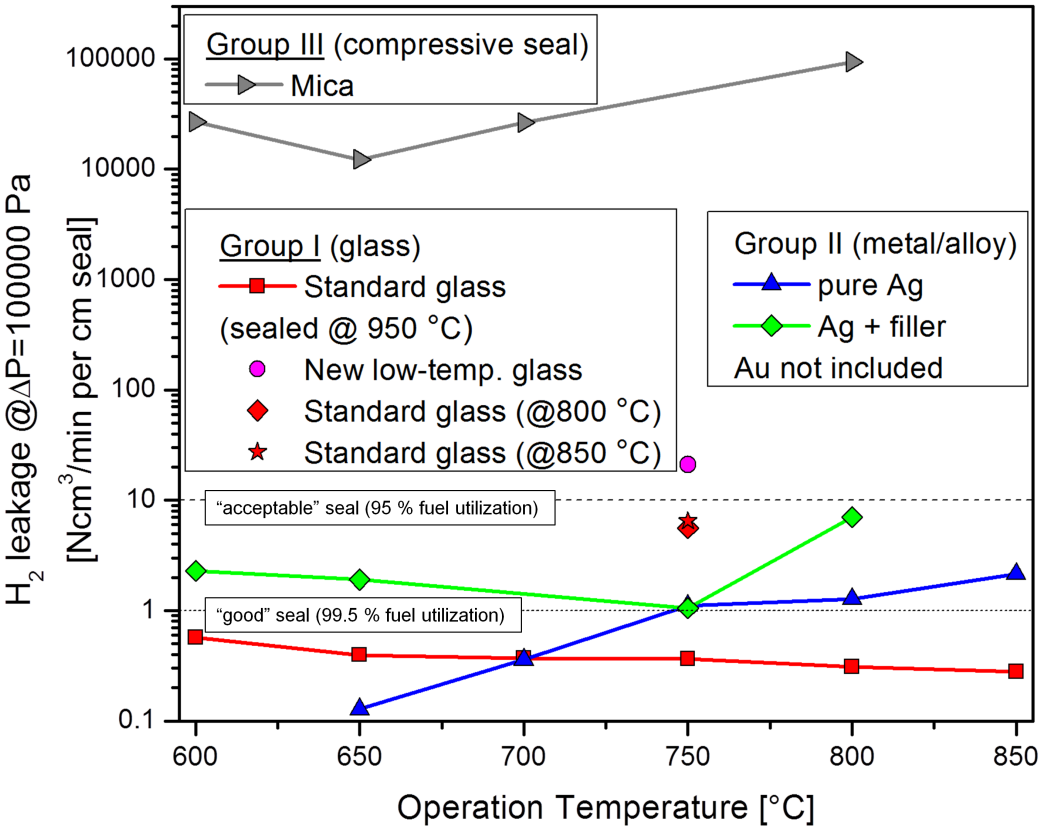


Figure 34. Selected results from the leak test study carried out in the project.

Another important part of the work done at IRD is related to the improvement and fabrication of standard auxiliary test components. The coupling layers produced by IRD have in this project served as a base-line supply for the single cell tests of anode-supported SOFCs. More than 100 coupling layers (contact components) of each type (Ni-YSZ and LSM) have been provided by IRD to Risø DTU during the project, along with several kg of glass powder used to manufacture glass sealant bars for cell tests.

### *1.4.5 Work Package 4 - Cell and Materials Characterisation*

#### 1.4.5.1 Development of a simplified method for nano-scale analysis of SOFC electrodes

The aim of this task was to capitalise on the increased spatial resolution gained by using TEM type "thin" samples. The work presented in this section was carried out to meet milestone M.4.1 "Development and demonstration of a method for nano-scale analysis of SOFC electrodes using FIB-FEG-SEM".

In the SEM electron beam accelerating voltages up to 30 kV are typically used for microanalysis by energy dispersive x-ray spectroscopy (EDS) on bulk samples. In this case the size of the electron beam interaction volume and not the electron beam diameter determines the spatial resolution of the chemical information. The electron beam interaction volume increases with increasing accelerating voltage and on average the chemical information has a spatial resolution on the order of 1 µm. In the TEM thin samples are used, where thin is defined by being significantly thinner than the depth of the interaction volume. Thus the combination of small beam diameter, high accelerating voltage and the absence of bulk material can result in chemical spatial resolution in the order of a few nm.

Initial work started by examining conventional TEM samples in the SEM in order to investigate spatial resolution and signal to noise / background relationships. The first experiment on an SOFC anode revealed that it was important to mount the sample in such a way that contaminating x-ray signals from the specimen mounting did not interfere with the EDS spectra. It could be concluded that the anticipated increase in spatial resolution could be achieved with such thin samples in the SEM. This first study was performed on a standard lift-out TEM sample which requires significant preparation time and effort contrary to the aims of developing a cheap and high resolution chemical analysis method.

In order to remove the time consuming process of performing in-situ TEM sample lift-out in the FIB-SEM an H-bar geometry sample was tested for its suitability for high resolution SEM EDS. A H-bar sample is a mechanically thinned sample of approximately less than 50 µm in thickness from which two regions are FIB milled from either side leaving a thin window suitable for investigation in the centre of the mechanically thinned section. Such samples are called H-bars due to their similarity in appearance to the letter "H" when viewed from above.

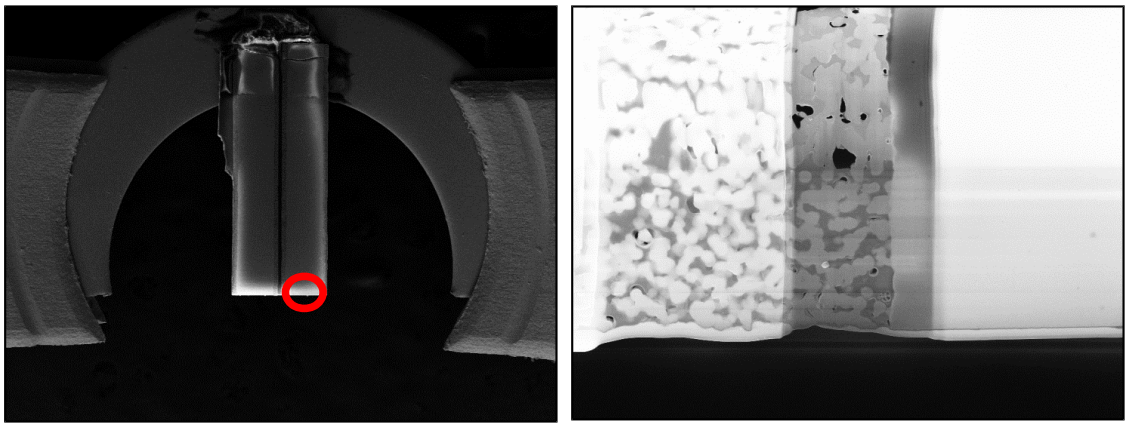

Figure 35: Left – a low magnification of an H-bar sample. The sample consists of two pieces of symmetric cell glued to each other which is then sectioned and mechanically thinned to less than 50 µm in thickness. The two samples can be seen oriented vertically in the centre of the image. The sample is then glued to a standard 3 mm half ring TEM sample holder (Cu) which is then clamped to an ion milling sample holder. Right – a higher magnification image of the FIB thinned section in the red circle in left hand image. The image contains the electrode/electrolyte interface. The porous solid oxide electrode is seen on the left and the dense ceramic electrolyte on the right.

The horizontal line in the H represents a top view of the thin section. In order to reduce interfering signals from the thick surrounding parts of the H-bar sample the method was modified to create an asymmetric H-bar such that the thin section is raised to the top of the sample with respect to the incident electron beam such as "∏". An overview of the H-bar sample is given in figure 35.

Based on the experiments conducted it could be concluded that using H-bar geometry samples is a successful approach. This means that much of the time consuming sample preparation for the first sample can now be avoided by using cheaper and simpler mechanical polishing methods, and the primary objectives in milestone M4.1 have been met despite the fact that the methods used are more complicated than originally planned. The method as it stands constitutes a bridge between conventional SEM EDS and high resolution TEM EDS and as such is now available as an investigation technique for SOFC material investigations. In comparison to conventional SEM bulk sample EDS analysis whose spatial resolution is approximately 1 µm, it can be concluded that the current technique offers approximately an increase in resolution of an order of magnitude.

#### 1.4.5.2 Development of software for batch analysis of SEM images of electrode microstructure

A key prerequisite to being able to assess the evolution of electrode microstructure during operation of SOFCs is to be able to accurately measure important microstructure parameters, *e.g.*, interfacial areas between phases, phase fractions (*e.g.* porosity) or particle size distributions. Scanning electron microscopy (SEM) images of electrode cross-sections are typically used to characterize the microstructure. However, the characterization task itself is often time consuming. This means that in practice the microstructure assessment is often done qualitatively or on only a small part of the sample. The project has contributed to the ongoing development of software (co-funded by the project "SOFC-LIFE" - project # FCH JU 526885 ) for easy characterization of electrode microstructure in a quantitative way. The idea behind the software is to make it easy to extract microstructure parameters from a large number of images quickly and in a reproducible way. This will enable the user to not only measure a given microstructure parameter accurately but also to assess the variability of that parameter. Thus, providing more accurate confidence intervals and enabling statistical hypothesis testing.

SEM images of electrode microstructure are the basic input to the software program. On many modern SEMs it is possible to program the microscope to acquire a series of images automatically with the same imaging conditions, *e.g.* along the electrolyte. To compare the microstructure between two different samples a series of images is produced from each sample.

The software makes it possible to load, inspect and organize these series of images such that a batch processing of all series and images can be carried out in one go. A screen shot of the program with its main windows open can be seen in figure 36.

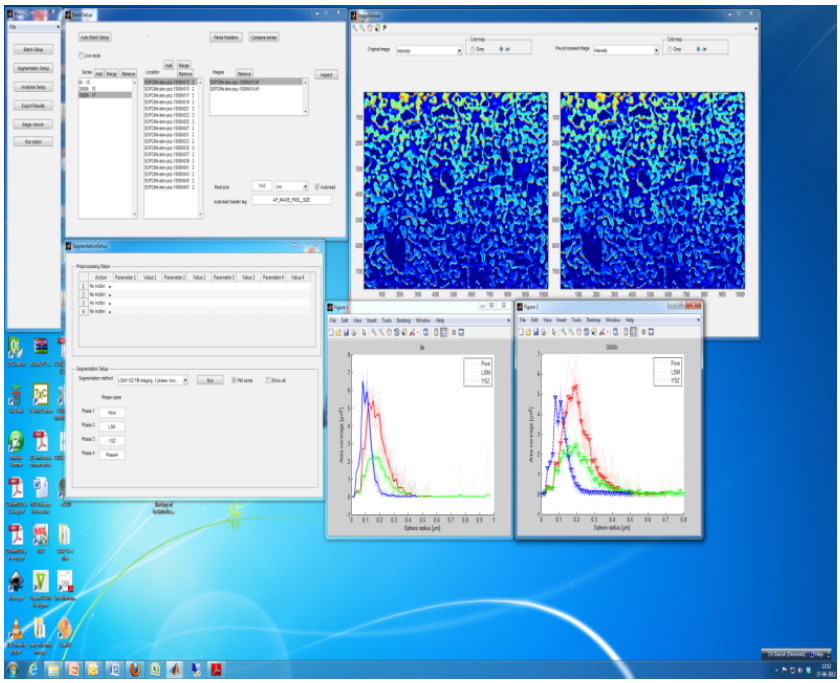

Figure 36. A screenshot of the program under development for microstructural analysis with the main windows open.

A number of methods for calculating microstructure parameters from the segmented images are implemented in the software. These parameters include phase fractions, interface areas between all phases, triple phase boundary length and different approaches to quantifying the distribution of the size of agglomerates and cavities. Functionality to present and export the results of the analysis is currently being worked on. The analysis of a typical image takes 10-100 s dependent on which segmentation method is used and which analysis options are selected. A whole batch of multiple series of multiple images can be processed without user intervention once the segmentation method has been set up.

In its current state the core functionality is implemented and the software is currently being used for batch analysis of microstructure. Additional testing and implementation of additional features is still ongoing. The software has been implemented in Matlab™ but can be deployed to run without having Matlab™ installed.

Further testing and tuning of the program is still needed but tests so far indicate that the program could make it much more practically feasible to do systematic quantitative studies of microstructure changes, *e.g.* resulting from altering of manufacturing parameters or from degradation during continued operation of SOFCs.

### 1.4.5.3 A method for screening of suitable SOFC cathode materials

A fast screening method for suitable cathode materials and their stability was developed in a Master of Science project (J. Højberg, "Screening of Suitable SOFC Cathode Materials", 2011) supported by the project. Testing of degradation of cathodes on solid oxide fuel cells is a very time consuming (and expensive) process. A fast screening method of cathode materials that can be utilized for degradation studies and in quality control is therefore highly desirable.

The developed method utilizes that mixed ionic electronic conductors (MIECs) which are typically used as oxygen reduction catalyst in SOFC cathodes, exchange oxygen with the surrounding atmosphere, when the oxygen partial pressure, $pO_2$, changes. The present method

employs a packed bed geometry, where the cathode material that needs to be investigated is placed in an alumina tube.

A gas is flowed through the powder sample and the $pO_2$ and flow downstream is measured. Figure 37 a) shows a schematic of the design. By changing the $pO_2$ that is flowed through the powder the MIEC inside the tube will adjust its oxygen stoichiometry as to be in equilibrium with the new $pO_2$. By monitoring the $pO_2$ and flow downstream of the powder it is possible to give quantitative estimates on the oxygen exchange reaction. The advantage of the developed method is a very rapid screening of the materials with a direct measurement of the process that takes place during cathode operation, however, this is done ex-situ a fuel cell, but it utilizes powder resembling the particles used in a SOFC cathode. The developed method has been used to *i*) Quantify the oxygen exchange reaction on powders sintered at different temperatures *ii*) Quantify how impurities in the gas phase effects the oxygen exchange reaction *iii*) Establish if powder received from a given supplier gives a unique 'fingerprint'. Figure 37 b) shows the $pO_2$ downstream of the sample after a rapid change in the oxygen partial pressure where the powder is $Ba_{0.5}Sr_{0.5}Co_{0.2}Fe_{0.8}O_{3-\delta}$ (BSCF). BSCF is considered to be used as a cathode material and is known to be highly catalytic active but also degrade very fast. The different legends illustrate the number of minutes the powder has been subjected to a $CO_2$ gas stream before the rapid change in $pO_2$. It is seen that exposure to $CO_2$ changes the response of the powder indicating that the powders goes from being a highly active oxygen reduction catalyst to a powder that does not respond significantly to a change in $pO_2$.

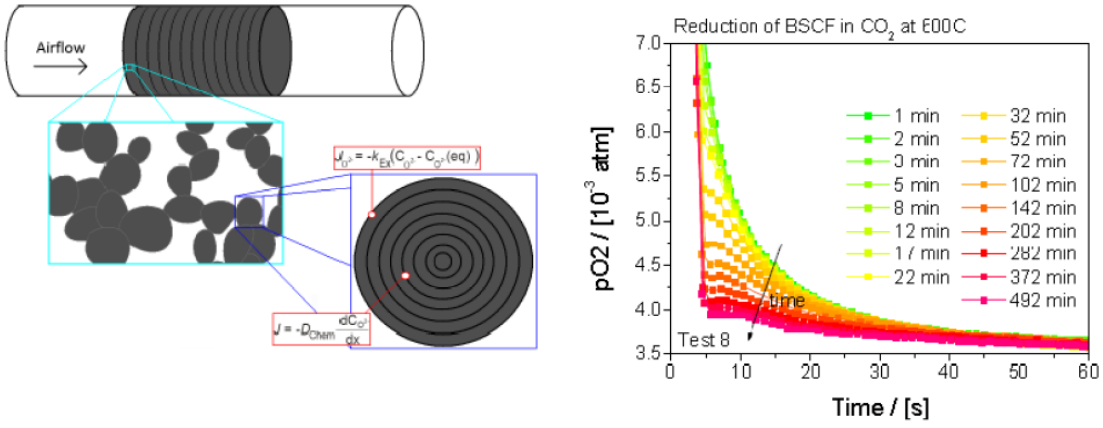


a) b)

Figure 37 a) Schematic of the screening method method. A flow of gas with a well defined oxygen partial pressure is flowed through the powder sample. A rapid change in the $pO_2$ causes the MIEC to equilibrate with the new $pO_2$. The equilibration is measured downstream of the powder. b) Example of investigation of $Ba_{0.5}Sr_{0.5}Co_{0.2}Fe_{0.8}O_{3-\delta}$ subjected to different times of CO2.

This clearly suggest that BSCF is a material that should be used with great care at 600 °C as $CO_2$ from the atmosphere can react with the powder. A similar analysis of LSCF did not show any changes in the kinetics with addition of $CO_2$, which is consistent with a higher thermodynamic stability of this material. With continued development it is considered that the method can be used in quality control of the cathode powder that is being used in commercial production of SOFCs.

### *1.4.6 Work Package 5 - Thermodynamic Calculations and Electrode Modelling*

#### 1.4.6.1 Thermodynamic stability of LCN

Work package 5 included an effort to establish thermodynamic stability of cathode materials suitable for low temperature operation (600 – 750 °C). Such cathode materials include LSC, LSCF, LCN etc. It is planned to investigate the phase stability of the cathode materials on their own and in contact with other cell component materials as a function of composition, temperature and oxygen partial pressure. The chosen methodology was CALPHAD, which stands for CALculation of PHAse Diagrams. The work demanded a self-consistent thermodynamic database including the following elements: La-Sr-Co-Fe-Ni-Cr-Ce-Gd-Y-Zr-O. An effort on developing a thermodynamic database of La-Sr-Co-Fe-O and on evaluation thermodynamic stability of LSCF cathode is currently being carried out in a concurrent PhD project. Results obtained in a previous project (ForskEL/PSO 2007-1-7124) on the performance of LCN – $La(Co,Ni)O_3$ used in composite SOFC cathodes showed excellent performance.[12] The stability of LCN is however not well studied. In the current project, LCN was chosen as the working subject for WT5.1. A thermodynamic database of La-Co-Ni-O was developed using the CALPHAD methodology. Thermodynamic calculations were then carried out to clarify stability of LCN cathode as a function of temperature, Co/Ni ratio, and oxygen partial pressure.

During the project period, work was carried out on developing thermodynamic databases of La-Co-O, La-Ni-O, Co-Ni-O, and La-Co-Ni-O. The thermodynamic database of La-Co-Ni-O was then developed based on the databases of La-Co-O, La-Ni-O, and Co-Ni-O. Phase diagrams were calculated at 600, 800, 1000, and 1200 °C .

The red triangle represents a 3-phase region, where the 3 corner points represent the compositions of the three phases in equilibrium. The green lines are the so-called tie-lines for 2-phase regions, where the two end-points of a single tie-line represent the compositions of the two phases in equilibrium. The $La(Co,Ni)O_3$ perovskite phase is stable over the entire composition range from $LaCoO_3$ to $LaNiO_3$ at 800 °C or lower temperatures. The Ni-rich side of the LCN perovskite becomes unstable with increasing temperature and it decomposes into a less Ni-rich perovskite, (Co,Ni)O, and the Ruddlesden-Popper phases.

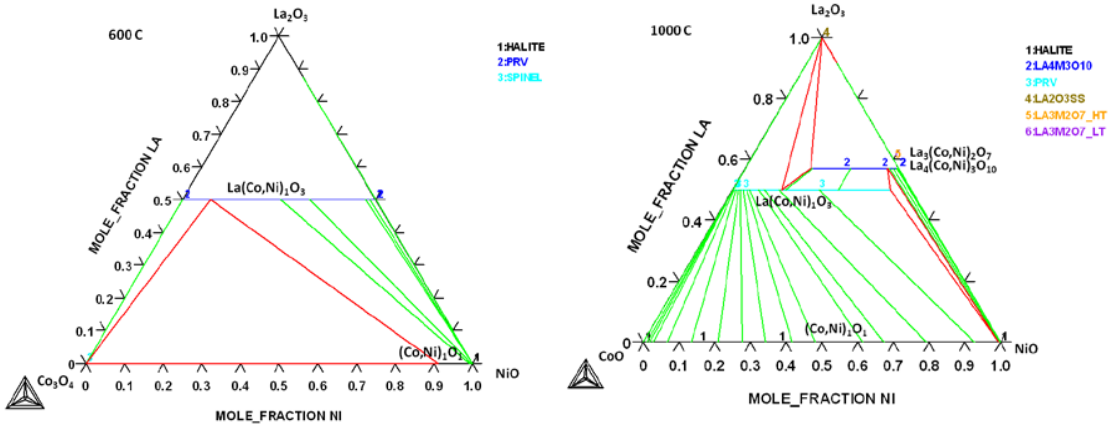


Figure 38: Calculated phase diagrams of $La_2O_3$-CoO-NiO at 600 and 1000 °C in air. Left: at 600 °C. Right: at 1000 °C.

Based on the current work, it can be concluded that the LCN perovskite has a rather limited stability range, which is influenced by Co/Ni ratio, temperature and oxygen partial pressure. As a cathode material, LCN is in principle suitable for application at low temperature and low

[12] P. Hjalmarsson and M. Mogensen, *Journal of Power Sources*, **196**, 7237–7244 (2011)

cathode polarization. High temperature or high cathode polarization may result in decomposition of LCN.

### 1.4.6.2 Clarification of the origin of degradation based on impedance models

In order to improve the understanding of the degradation on both cells and model electrodes, different impedance models have been developed. The main focus was placed on the development of a physically reasonable impedance model of the anode response, as this is one of the components in the fuel cells that often shows the greatest total degradation, and the largest degradation rate at short times (< 1000 h). The developed impedance model was subsequently combined with a microstructural model, in order to quantify the effects on the impedance as a function of changing microstructural parameters in the anode. Specifically, this work investigated how the impedance of anodes should evolve as a function of time, assuming that nickel coarsening is the only factor contributing to the degradation.

A detailed study by M. Pihlatie et al. investigated the electrical conductivity as a function of time for typical anode structures used at DTU.[13] These data have been evaluated with a microstructural model in order to predict an average particle size, as well as triple phase boundary length changes with time.[14] Assuming that the decrease in conductivity with time can be attributed to coarsening of Ni, it is possible to correlate the measured conductivity to the particle size of Ni, and subsequently calculate the triple phase boundary length.

In order to predict how the impedance will evolve as a function of changing microstructural parameters, it is necessary to describe how a reduced triple phase boundary affects the impedance. This can only be achieved with an accurate model. In this work, a modified form of a model utilized by Sonn et al. was used.[15] Figure 1 b) shows Nyquist plots at 850 °C, 20 and 40 % $H_2O/H_2$ for a Ni/8YSZ anode and a modified Ni/3YSZ anode support in a symmetric cell configuration. The impedance response consist in principle of the anode electrochemistry part (including ionic transport and charge transfer processes), the gas transport in the anode support (seen at the lowest frequencies) and gas transport in a stagnant gas layer above the electrode (also seen at the lowest frequencies), as described by other authors.[15,16]

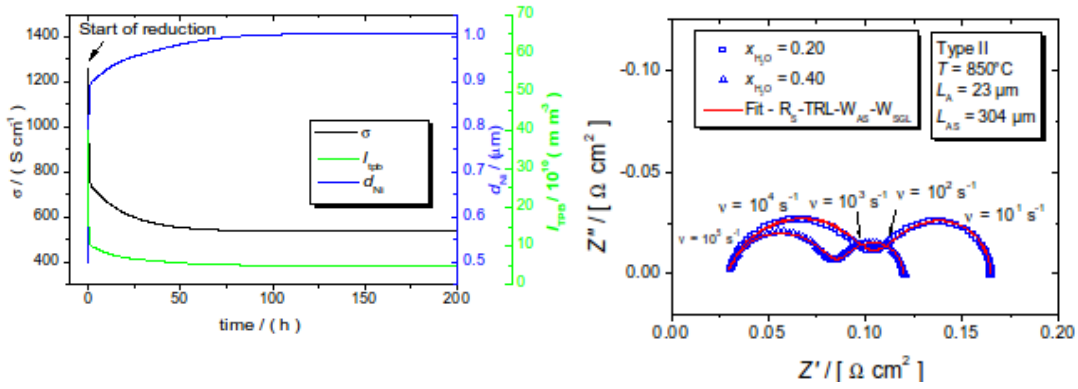


Figure 39. Electrical conductivity (left axis), particle size of Ni (inner right axis) and triple phase boundary (TPB) length (outer right axis) as a function of time. b) Measured impedance spectra of Ni/8YSZ. Notice that the impedance spectra are recorded at two different steam contents. The impedance spectra have been fitted using a modified version of the model described in Ref. 3 for the electrochemical part of the electrode response, in addition to two Warburg impedances representing a stagnant gas layer above the electrode, as well as gas transport through the anode support.

[13] M. H. Pihlatie, A. Kaiser, M. Mogensen, and M. Chen, Solid State Ionics 189(1) 82-90 (2011).

[14] J. H. Nam and D. H. Jeon, Electrochimica Acta, 51(17) 3446-3460 (2006).

[15] V. Sonn, A. Leonide, and E. Ivers-Tiffee, Journal of The Electrochemical Society, 155(7) B675-B679 (2008).

[16] T. Ramos, K. Thydén, M. Mogensen, ECS Transactions, 29 (2010) 123.

The fit to the developed model is seen as the red line. Very good agreement was obtained between the measured and fitted data for a series of relevant impedance spectra.

The quantification of the charge transfer resistance, allowed by the fitting, in addition to the predicted particle sizes from the electrical conductivity studies, makes it possible to make a quantitative estimation of how the anode impedance evolves as a function of nickel coarsening. The result is exemplified in figure 40 a), which shows predicted impedances at several times using the developed model combined with the values based on the electrical conductivity measurements. Figure 40 b) shows the corresponding Bode type plots.

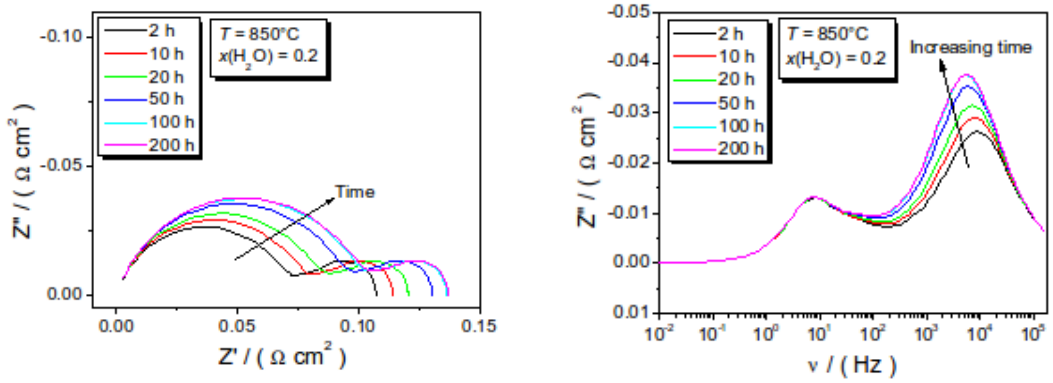


Figure 40: a) Nyquist plot of predicted impedances for different times. The times listed in the legend correspond to the times given in Figure 39 a). b) Bode type plot of the impedance spectra shown in a).

From the modelling it can be concluded that for Ni-coarsening the main change in the frequency range will be in the range from 20 kHz to 500 Hz. Of other possible degradation mechanisms of the anode can be *i*) hindered gas transport in the anode structure and *ii*) a decrease of the effective ionic conductivity in the (ionic) backbone. If gas transport is hindered this will be seen at low frequencies whereas if the ionic transport in the backbone is hindered this will mainly be seen at frequencies above 10 kHz.

### *1.4.7 Dissemination of Project Results*

The work conducted in this project has resulted in a number of public presentations in the form of poster or oral presentations, and scientific articles in peer-reviewed journals. These contributions are listed below:

*Publications:*

1. "Ni/YSZ anode - Effect of pre-treatments on cell degradation and microstructures", A. Hauch, P. S. Jørgensen, K. Brodersen and M. Mogensen, *Journal of Power Sources* (Elsevier), 196 (2011) 8931–8941.
2. "Durability of Solid Oxide Cells", R. Knibbe, A. Hauch, J. Hjelm, S. Ebbesen, M. Mogensen, *Green* (De Gruyter), Vol. 1 (2011), pp. 141–169
3. "Highly durable anode supported cells with LSC-based infiltrated cathode", A. J. Samson, P. Hjalmarsson, M. Søgaard, J. Hjelm, and N. Bonanos, *Journal of Power Sources* (Elsevier) **216**, 124–130 (2012).
4. "Impact of Reduction Parameters on the Initial Performance and Stability of Ni/(Sc)YSZ Cermet Anodes for SOFCs ", S. L. Ebbehøj, T. Ramos, and M. Mogensen, ECS Transactions, 2012, Volume 45, Issue 1, pp. 363-375
5. "Durability and Performance of High Performance Infiltration Cathodes " M. Søgaard, A. J. Samson, N. Bonanos, J. Hjelm, P. Hjalmarsson, S. P. V. Foghmoes and T. Ramos . Proc. European Fuel Cell Forum, 2012, A1002, Lucerne

*Oral and Poster Presentations:*

6. J. Bowen, Presentation at "Workshop on Image Analysis in SOFC Degradation Research", held at Research Centre Juelich, Juelich, Germany, September, 2010
7. K. Thydén, T. Ramos, M. Mogensen, "Visualization of the Electronic Conducting Path in a Solid Oxide Fuel Cell by Low-voltage SEM and Charge Contrast", Poster presentation M21513; IMC-17 – International Microscopy Congress, Rio de Janeiro, Brazil, September, 2010
8. A. Hauch, "Impurity related degradation of SOFC Ni/YSZ electrodes" , Oral presentation at Fuel Cells Science and Technology Conference, Grove Event, Zaragoza, Spain, October, 2010
9. P. Hjalmarsson, "Sintering of $La_{0.6}Sr_{0.4}CoO_3$ cathodes and its correlation to electronic conductivity and electrochemical performance". Poster Presentation at "ECerS XII" (12th Conference of the European Ceramic Society), Stockholm, Sweden, June 19-23, 2011
10. A. Hauch, "Impedance spectroscopy characterization of high performing SOFC with Ni/ScYSZ anode", Presentation at "Electrochemical Frontiers in Global Environment and Energy, 11-16 September, 2011, Niigata, Japan" (62nd Annual Meeting of the International Society of Electrochemistry).
11. J. Hjelm "Degradation Testing – Quantification & Interpretation", Presentation at the 2nd International Workshop on Degradation Issues of Fuel Cells, Thessaloniki, Greece, 21-23 September, 2011
12. C. Graves "Determination of overpotential characteristics of reversible solid oxide cells via impedance spectroscopy", Presentation at the 220th meeting of the Electrochemical Society, Boston, USA, October 11th, 2011
13. J. J Bentzén, K. T. S. Thydén, J. R. Bowen, W. Zhang, E. Abdellahi, "Optimization of Analytical SEM for Ceramic Energy Materials Research", Poster at the Annual Meeting of the Nordic Microscopy Society (Scandem), Bergen, Norway, 12-15 June 2012

The project results are further documented in confidential technical reports, and a number of manuscripts intended for publication in the near future.

### *1.4.8 Environmental Benefits of the Project*

Denmark is committed to contribute to limit the global climate change as agreed in Copenhagen 2009 and in Cancún 2010. One integral part of this commitment is the reduction of greenhouse gas emissions in Europe by 80-95% in 2050 compared to the 1990 level.
This project contributes indirectly to achieving this goal by carrying SOFCs further to a technology break through, where the inherent advantages of SOFCs can be utilised:

- Decrease the emission of CO2 due to the higher system efficiencies
- Easier and cheaper carbon capture and further processing, as $CO_2$ is produced in concentrated form and not diluted by huge amounts of air
- Avoidance of $NO_x$ and $SO_2$ emissions, as these compounds are not formed in the SOFC process

## 1.5 Utilization of project results

The Danish roadmap and strategy 2010-20 sets out the development targets necessary for commercialization of the Danish SOFC technology. The results from the present project will play a key role in achieving these targets. The results, in particular improvements in cell performance and durability, improved understanding of degradation, and fruitful degradation mitigation strategies will be transferred to Topsoe Fuel Cell, in order to allow implementation

in cells used in stacks and systems. Furthermore, the results will be the basis for the necessary further research and development at DTU Energy Conversion.

## 1.6 Project conclusion and perspective

The key outcome of the project can be summarized in the following points:

- Better understanding of the importance of microstructural differences between cells versus the difference in properties of the ionically conducting ceramic phase in Ni-cermet electrodes
- A promising strategy for improvement of impurity tolerance (chemical robustness) of Ni-cermet electrodes in the form of nanostructured coatings
- Better insight into the impact of initial reduction of the Ni-cermet electrodes on their performance and stability, which is important for obtaining the best possible performance and durability from different types of cells.
- A first assessment of the long-term stability of a cell with a nanostructured oxygen electrode, which also indicates that highly stable cells can be manufactured with such electrodes.
- Development and integration of LSC-based cathodes yielding excellent performance and promising long-term stability. The sensitivity of this cathode to moderate amounts of water vapour in the oxidant gas stream was shown to be very low.
- Incorporation of state-of-the-art data validation and analysis techniques, including physical models not available in commercial software for impedance data analysis, into software suitable for handling large amounts of data.
- An improved description of degradation by detailed electrochemical characterization of cells operated at 0.5 - 0.75 $A \cdot cm^{-2}$ at 700 °C, in which the degradation (i.e. the change in performance) could be followed component or process-wise for periods of up to 3000 h.
- Quantified degradation rates for the Ni-YSZ anode, YSZ electrolyte, and both LSCF-CGO, LSC, and LSC-CGO cathodes
- Improved understanding of factors controlling RedOx stability of anode-supported SOFCs
- An initial investigation of the evolution of the mechanical properties of anode-supported cells during aging in a simulated stack environment (aging in high water content fuel) where the mechanical testing was carried out at operating temperature.
- A simple manufacturing method for sealant frames suitable for for use in single cell testing at lower start-up temperatures
- Development of a simplified method for nano-scale analysis of SOFC electrodes
- A thermodynamic database for $La(Co,Ni)O_3$ perovskite materials and an assessment of the thermodynamic stability of this material in the context of its' use as a SOFC cathode
- An impedance model combined with a microstructural model that yields insight into expected changes of the impedance response of Ni-YSZ electrodes as they undergo degradation due to Ni-coarsening.

With a long-term degradation of the YSZ electrolyte and the Ni-YSZ anode of approximately 2 mΩ·cm2 per 1000 h, and a cathode degradation of approximately 1-2 mΩ·cm2, gives a total degradation rate of about 6 $m\Omega \cdot cm^2$ per 1000 h (without any changes in the gas concentration impedance), as measured using impedance spectroscopy. The lowest overall long-term degradation rate as measured from the cell voltage (at operating times exceeding 1000

h) was approximately 8 mΩ·cm$^2$ per 1000 h in good agreement with the long-term degradation rate obtained from impedance spectroscopy measurements.

The 2015 target in the National Danish SOFC Roadmap (September 2010) for cell performance is an ASR of 0.22 Ω·cm$^2$ and a degradation rate of 0.66% / 1000 h. The resistance change over time calculated from a cell voltage (or power) degradation of 0.66% / 1000 h depends on current density and cell resistance. For a cell with an initial resistance of 0.22 Ω·cm2 (220 mΩ·cm$^2$) running at a current density of 0.5 A cm$^{-2}$ (with an open circuit voltage of 1.1 V) this corresponds to approximately 13 mΩ·cm$^2$ per 1000 h of operation. The commercial (CHP) system target degradation rate is 10% degradation over 40000 h with natural gas as fuel. The 2020 target value for cell performance is 0.18 Ω·cm$^2$. Taken together this gives a degradation rate in the range 4 – 5 mΩ·cm$^2$ per 1000 h of operation at a current density of 0.5 A cm$^{-2}$. Higher current density requires even lower degradation rates e.g. for operation at 1.0 A cm$^{-2}$ the degradation rate must be maintained at less than 2.5 mΩ·cm$^2$ per 1000 h to reach the 2020 cell voltage degradation target.

The long-term degradation rates of the cells investigated in the project were in the range 6 – 16 mΩ·cm$^2$ per 1000 h and represents the intrinsic degradation rate of the cell, which is unavoidable, and was obtained under steady-state conditions. This does not include extrinsic degradation (*e.g.* impurities in fuel or oxidant gas), degradation due to transient conditions, thermal cycles etc. Although the results indicate that there is little room for extrinsic degradation, these are promising results with respect to durability. The ASR is still too high with respect to the 2020 target. The outcome of this project provides guidelines for the future focus of development in order to achieve increased performance, better durability, and more cost-efficient anode-supported solid oxide fuel cells.